
UAMTERS: UNCERTAINTY-AWARE MUTATION ANALYSIS FOR DL-ENABLED ROBOTIC SOFTWARE

Chengjie Lu

Simula Research Laboratory and University of Oslo
Oslo
Norway
chengjielu@simula.no

Jiahui Wu

Simula Research Laboratory and University of Oslo
Oslo
Norway
jiahui@simula.no

Shaukat Ali

Simula Research Laboratory
Oslo
Norway
shaukat@simula.no

Malaika Din Hashmi

Danish Technological Institute
Odense
Denmark
mdih@teknologisk.dk

Sebastian Mathias Thomle Mason

Danish Technological Institute
Odense
Denmark
sem@teknologisk.dk

Francois Picard

Danish Technological Institute
Odense
Denmark
fpi@teknologisk.dk

Mikkel Labori Olsen

Danish Technological Institute
Odense
Denmark
miol@teknologisk.dk

Thomas Peyrucain

PAL Robotics
Barcelona
Spain
thomas.peyrucaain@pal-robotics.com

ABSTRACT

Self-adaptive robots adjust their behaviors in response to unpredictable environmental changes. These robots often incorporate deep learning (DL) components into their software to support functionality such as perception, decision-making, and control, enhancing autonomy and self-adaptability. However, the inherent uncertainty of DL-enabled software makes it challenging to ensure its dependability in dynamic environments. Consequently, test generation techniques have been developed to test robot software, and classical mutation analysis injects faults into the software to assess the test suite’s effectiveness in detecting the resulting failures. However, there is a lack of mutation analysis techniques to assess the effectiveness under the uncertainty inherent to DL-enabled software. To this end, we propose *UAMTERS*, an uncertainty-aware mutation analysis framework that introduces uncertainty-aware mutation operators to explicitly inject stochastic uncertainty into DL-enabled robotic software, simulating uncertainty in its behavior. We further propose mutation score metrics to quantify a test suite’s ability to detect failures under varying levels of uncertainty. We evaluate *UAMTERS* across three robotic case studies, demonstrating that *UAMTERS* more effectively distinguishes test suite quality and captures uncertainty-induced failures in DL-enabled software.

Keywords Self-adaptive Robotic System · Mutation Analysis · Uncertainty Quantification · Deep Learning

1 Introduction

Self-adaptive robots are designed to handle unexpected situations and make decisions in response to unpredictable environmental changes. Such systems have shown great potential in safety-critical domains, including autonomous driving [1], industrial automation [2], and maritime [3], where operating conditions are highly dynamic and unpredictable at runtime. In recent years, the use of deep learning (DL) components in self-adaptive robotic software has increased, as they enable advanced perception, decision-making, and control, thereby enhancing autonomy and adaptability. Meanwhile, integrating DL into robotic software increases complexity, making it more challenging

to ensure dependability in unpredictable environments. Moreover, DL models inherently exhibit various forms of uncertainty arising from factors such as limited training data and stochastic inference mechanisms (e.g., prediction-time dropout) [4], further complicating the validation of robot behavior at runtime.

To ensure the dependability of robotic software, various testing techniques have been proposed [5]. However, there is a lack of mutation analysis approaches for assessing the quality of generated test suites, particularly from the perspective of their ability to deal with the inherent uncertainty of DL components in robotic software. Such mutation analysis techniques help evaluate the ability of test suites to reliably detect safety and performance violations under realistic and uncertain conditions. Various mutation analysis approaches have been proposed for DL-enabled robotic software. For example, DeepMutation [6] and DeepMutation++ [7] inject faults into DL models using novel mutation operators and can be applied across a wide range of DL architectures. Furthermore, DeepCrime [8] integrates 35 mutation operators derived from the analysis of real DL faults, enabling the simulation of real faults in DL models. In addition, Jahangirova and Tonella [9] conduct an empirical evaluation to identify effective mutation operators and propose a statistical definition of mutation killing, further supporting rigorous mutation testing of DL-enabled systems.

While the above works advance mutation analysis for DL-enabled software, they do not explicitly consider the uncertainty inherent in DL models. Uncertainty arising from limited training data, dropout, and stochastic inference mechanisms can significantly affect robot behavior, particularly in complex and unpredictable operating environments. As a closely related work, DeepCrime [8] introduces a mutation operator that modifies dropout layers; it treats dropout as a training-time regularization technique rather than as a mechanism for characterizing predictive uncertainty during inference. Therefore, there is a need for mutation analysis techniques to assess the ability of test suites to detect failures arising from uncertainty in DL components within robotic software.

To address this limitation, we propose *UAMTERS*, an uncertainty-aware mutation analysis framework, for DL-enabled software in robots. *UAMTERS* proposes novel operators that inject uncertainty into DL models, enabling systematic simulation of uncertain model behaviors to assess the test suite’s ability to reveal failures caused by these behaviors. We quantify this with novel uncertainty-aware mutation score metrics. By explicitly accounting for uncertainty, *UAMTERS* enables a more informative evaluation of test suite quality in revealing failures caused by uncertainty. We evaluate *UAMTERS* using three industrial-level robotic case studies, comprising seven embedded DL models and eight test suites. The results show that our novel mutation score metrics are more effective in distinguishing test suite quality than traditional mutation scores. Moreover, the proposed mutation score metrics capture model degradation by tracking changes in uncertainty.

In summary, our contributions are: 1) *UAMTERS*, an uncertainty-aware mutation analysis framework for DL-enabled robotic software integrating novel uncertainty-aware mutation operators to explicitly inject stochastic uncertainty into robot behaviors; 2) Novel uncertainty-aware mutation score metrics that quantify a test suite’s ability to reveal model degradation and behavioral changes under varying levels of uncertainty; 3) Extensive empirical evaluation across industrial-level robotic case studies, demonstrating that the proposed mutation score metrics more effectively distinguish test suite quality and capture uncertainty-induced model performance degradation.

2 Context and Background

2.1 Context: RoboSAPIENS European Project

RoboSAPIENS [10] is a large European initiative focusing on building open-ended, safe, and trustworthy self-adaptive robotic systems. It extends the well-established self-adaptation framework, the MAPE-K loop [11], to ensure safe and reliable robot behaviors during operation time. A typical MAPE-K loop consists of five components: the Monitor component continuously observes the system’s state, while the Analyze component processes this state information to identify potential needs for adaptation. When adaptation is required, the Plan component generates an appropriate strategy, which is then executed by the Execute component. During this process, all components contribute to the Knowledge component, which stores relevant system information and historical data. The extended framework, referred to as the MAPLE-K loop (see Fig. 1), introduces an additional component called Legitimate, which validates the safety and performance of the robot’s planned actions before execution. A key consideration of Legitimate is the design of test suites that can effectively assess whether planned actions satisfy safety and performance requirements under uncertain and dynamic conditions. Although various test generation techniques have been proposed to evaluate the self-adaptive capabilities of robotic systems [12], existing approaches largely focus on generating test cases rather than assessing the quality of the resulting test suites. In this context, mutation analysis offers a systematic approach for evaluating test suite quality in self-adaptive robotic systems. By introducing controlled mutants into the system, it simulates realistic perturbations in robot behavior. This allows for the evaluation of how effectively a test suite can detect potential failures, supporting the Legitimate component in the MAPLE-K loop.

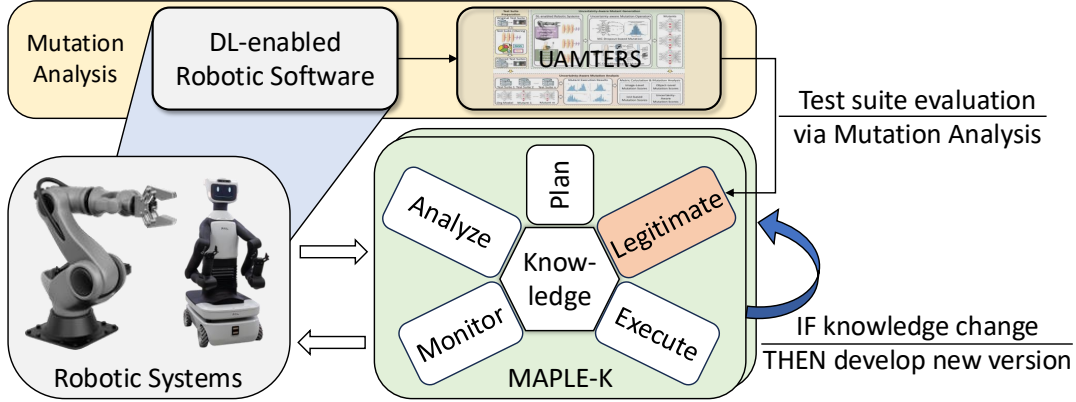


Figure 1: *UAMTERS* in the Context of the MAPLE-K Loop.

2.2 Uncertainty in Deep Learning

DL has shown significant success in fields such as computer vision [13], natural language processing [14], and robotics [15]. However, DL still faces major challenges in managing uncertainty, which can limit its reliability in real-world applications [4, 16]. Uncertainty in DL models is typically categorized into aleatoric uncertainty, which arises from inherent noise or randomness in the data (e.g., sensor errors or poor data quality), and epistemic uncertainty, which is caused by limited knowledge of optimal model parameters and commonly appears when the model encounters previously unseen data. Recent literature [17, 18] identifies uncertainty in DL as an important cause of failures in DL systems, leading to unreliable behavior in safety-critical applications. Uncertainty quantification (UQ) is essential for assessing the reliability and trustworthiness of DL models in real-world applications. To this end, various UQ approaches have been proposed, including Bayesian Neural Networks (BNNs) [19], MC-Dropout [20], MC-DropBlock [21], and Deep Ensembles [22]. BNNs provide a probabilistic framework to model uncertainty by applying Bayesian inference to DL models [19]; however, their practical application is often limited by the high computational cost and the complexity of posterior inference. As a result, several Bayesian approximation methods have been proposed to enable more efficient and scalable UQ. Gal and Ghahramani [20] introduce MC-Dropout, which approximates Bayesian inference by retaining dropout layers during inference and performing multiple stochastic forward passes. Building on this idea, MC-DropBlock [21] extends MC-Dropout to convolutional neural networks (CNNs) by randomly dropping contiguous regions in feature maps, thereby providing a more structured and effective UQ for CNNs.

Beyond UQ methods, designing effective UQ metrics is important for capturing uncertainties in DL models. Focusing on DL-enabled object detection software, Lu et al. [23] implement two categories of UQ metrics: UQ metrics for label classification and UQ metrics for bounding box regression. For classification tasks, three common metrics are used [4]: Variation Ratio (VR) [24], Shannon Entropy (SE) [25], and Mutual Information (MI) [25]. VR measures dispersion by calculating the proportion of predictions that differ from the most frequent class, SE quantifies the average information in the predictive distribution, and MI captures epistemic uncertainty by estimating the discrepancy between the predictive distribution and the posterior over model parameters. For bounding box regression, uncertainty is estimated using Total Variance (TV) [26] and Predictive Surface (PS) [27]. TV sums the variances of the box coordinates from the covariance matrix of the predicted boxes, while PS measures spatial uncertainty by computing the area of the convex hull enclosing the predicted bounding box corners.

In this work, we design two uncertainty-aware mutation operators based on the MC-Dropout and MC-DropBlock methods to explicitly inject stochastic uncertainty into DL-enabled software. To evaluate test suite effectiveness, we further propose novel uncertainty-aware mutation scores, calculated based on the UQ metrics employed by Lu et al. [23], which quantify the ability of test suites to reveal model degradation under different levels of uncertainty.

3 Methodology

3.1 Overview

Fig. 2 presents the workflow of *UAMTERS*, which adapts mutation analysis to DL-enabled robotic software. The workflow starts with *Test Suite Preparation* to filter out irrelevant test cases. Specifically, given an original test suite TS , *UAMTERS* executes the original DL model O on TS and keeps the set of passed test cases $TS' \in TS$ for mutation

analysis. After obtaining the *Filtered Test Suites*, the *Uncertainty-Aware Mutant Generation* begins, in which the DL-enabled robotic software is systematically mutated. In this work, a *Mutant* is defined as a variant of the original DL model obtained by applying an uncertainty-aware mutation operator, which injects stochastic uncertainty into the model at inference time. In detail, we generate mutants of the DL components using two mutation operators: MC-Dropout-based mutation (*MCD*) and MC-DropBlock-based mutation (*MCB*), which are introduced in Section 3.2. Finally, in the *Uncertainty-Aware Mutation Analysis* phase, we execute the original models and all their mutants on the *Filtered Test Suites* to evaluate the quality of the test suites based on the execution results.

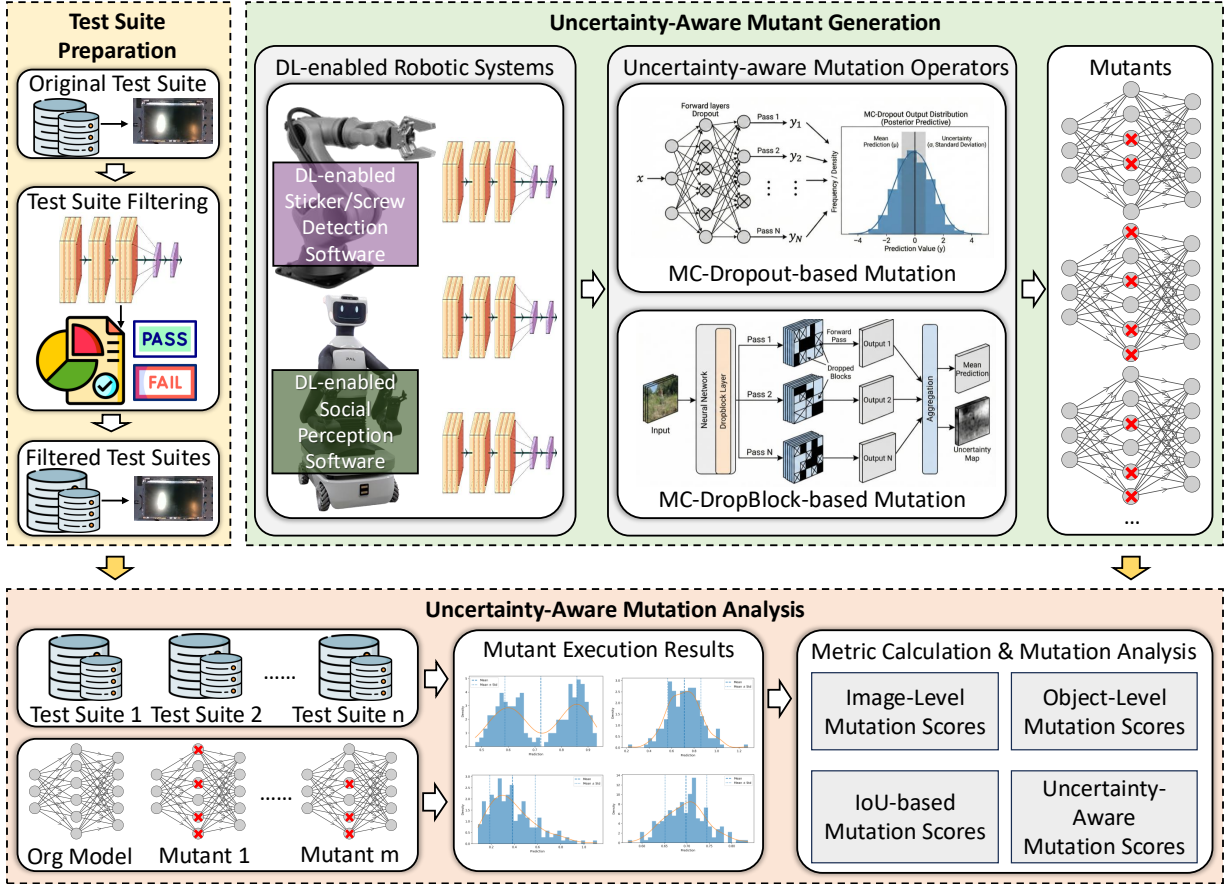


Figure 2: Overview of UAMTERS.

3.2 Uncertainty-Aware Mutation Operators

DL models may exhibit incorrect behavior due to various factors, among which uncertainty inherent in the model is an important cause, often leading to unstable or incorrect predictions [28, 29]. Motivated by this observation, we design two uncertainty-aware mutation operators to emulate failure scenarios caused by predictive uncertainty in DL. These operators generate mutants of the DL model by introducing uncertainty into the model, leading to deviations from correct predictive behavior, especially when the model is exposed to unseen input distributions.

3.2.1 MC-Dropout-based Mutation (*MCD*) Operator

MCD is a mutation operator that leverages the MC-Dropout method [20] to inject uncertainty into DL models. Since MC-Dropout effectively models uncertainty in DL as a Bayesian approximation, we employ it to design the *MCD* operator. Specifically, *MCD* works as follows: given a DL model O , *MCD* mutates the model by enabling dropout layers during inference time, resulting in a mutant:

$$MCD(O, \mu) = O_{\text{mcd}, \mu}, \quad (1)$$

where $O_{\text{mcd}, \mu}$ denotes the mutated network with inference-time dropout applied, and μ is the mutation ratio controlling the strength of the mutation. In *MCD*, μ specifies the probability that a neuron is dropped during inference; a higher

value of μ results in more neurons being dropped, thereby injecting greater uncertainty in the model and increasing the chance of uncertainty-induced failures. By adjusting this parameter, *MCD* can systematically control the amount of uncertainty injected into the model, enabling the study of model behavior under varying levels of uncertainty.

3.2.2 MC-DropBlock-based Mutation (*MCB*) Operator

MCB is a mutation operator designed based on the MC-DropBlock method [21], which was originally proposed to model uncertainty in object detection models. MC-DropBlock is specifically tailored for object detection models with convolutional layers, such as YOLO [30] and convolutional transformers [31]. Given that our subject systems are object detection models, we employ *MCB* to introduce uncertainty into the convolutional layers at inference time, thereby producing mutant models that may exhibit failures induced by predictive uncertainty. Specifically, given a DL model O , its mutant generated by *MCB* is:

$$MCB(O, \mu) = O_{\text{mcb}, \mu}, \quad (2)$$

where $\mu = [\mu_d, \mu_b]$ is a vector of mutation ratios: μ_d is the dropout rate controlling the probability of dropping individual neurons, and μ_b is the block size controlling the size of contiguous regions of neurons to be dropped. Large μ_d results in more individual neurons being dropped, while larger μ_b results in bigger contiguous blocks of neurons being dropped in the feature maps. Higher values of these mutation ratios increase the level of uncertainty injected into the model. By adjusting these two parameters, *MCB* can systematically control both the amount and spatial extent of uncertainty injected into the model, enabling the study of model behavior under different levels of uncertainty.

3.3 Mutation Scores

Mutation score quantifies the quality of a test suite by measuring how many generated mutants are killed by the test suite. A mutant is considered *killed* if at least one test case in the test suite produces an output that differs from the original model. For simple DL problems, such as classification and regression, the output is a single vector. When it comes to object detection models, the outputs become a set of bounding boxes, labels, and scores, making the definition of a mutant’s behavior change more complex. To address this challenge, we propose a set of novel mutation scores specifically tailored to object detection models. In particular, Section 3.3.2 introduces mutation score metrics defined at the object level, while Section 3.3.4 presents novel uncertainty-aware mutation scores. In addition, Section 3.3.1 defines the traditional mutation scores at the image level, which serve as a baseline for comparison with our proposed mutation scores. Before introducing these metrics, we first formalize the basic concepts required for mutation score calculation.

Definition 3.3.1 (Output of an Object Dection Model) *Given an object detection model ODM and a test input img, the output of ODM is a set of detected objects:*

$$O = ODM(\text{img}) = \{d_1, d_2, \dots, d_n\}, \quad (3)$$

where each detection $d_i = (b_i, c_i, s_i, u_i)$ consists of a bounding box coordinates (x_1, x_2, y_1, y_2) , a predicted class label c_i , and a class probability vector $p_i \in [0, 1]^K$, where each element represents the predicted probabilities over the K object classes.

Definition 3.3.2 (Match) *Given a test input img to an original ODM and its mutant ODM', let their outputs be O and O' . A pair $(d_i, d'_j) \in O \times O'$ is considered a Match if their bounding boxes sufficiently overlap and their labels are the same:*

$$\text{IoU}(b_i, b'_j) > \theta_{\text{IoU}} \wedge c_i = c'_j, \quad (4)$$

where b_i and b'_j denote the bounding boxes associated with detections d_i and d'_j , respectively, c_i and c'_j denote their corresponding predicted class labels, and θ_{IoU} is a predefined threshold. We set $\theta_{\text{IoU}} = 0.5$, following common practice in object detection tasks. Then, the set of all valid matches is denoted as:

$$\mathcal{S}_{\text{match}} = \{(d_i, d'_j) \in O \times O' \mid (d_i, d'_j) \text{ satisfies (2)}\}. \quad (5)$$

Definition 3.3.3 (Miss) *A detection d_i in the original output set O is defined as a Miss if it fails to find a valid counterpart in the mutant set O' within the set of matches \mathcal{M} . Formally, the set of Misses is defined as:*

$$\mathcal{S}_{\text{miss}} = \{d_i \in O \mid \forall d'_j \in O', (d_i, d'_j) \notin \mathcal{S}_{\text{match}}\}. \quad (6)$$

These represent objects correctly identified by the original model but missed by the mutant.

Definition 3.3.4 (Ghost) *A detection d'_j in the mutant output set O' is defined as a Ghost if it is not paired with any detection in the original set O within the set of matches \mathcal{M} . Formally, the set of Ghosts is defined as:*

$$\mathcal{S}_{\text{ghost}} = \{d'_j \in O' \mid \forall d_i \in O, (d_i, d'_j) \notin \mathcal{S}_{\text{match}}\}. \quad (7)$$

These represent false positives introduced by the mutation that were not present in the original model’s output.

3.3.1 Image-level Mutation Score

Image-level mutation scores measure test suite quality by capturing behavioral deviations between the original object detection model and its mutant models at the image (i.e., test case) level. In DL mutation analysis, a mutant is considered to be killed if its output differs from that of the original model. Further, to mitigate the effects of randomness inherent in stochastic model behaviors, Jahangirova and Tonella [9] introduced a statistical notion of mutation killing, in which a mutant is regarded as killed only when the output difference between the original model and the mutant is statistically significant. Therefore, we execute the original model and its mutant n times and define a mutant as killed under a test suite TS if the behavioral difference observed on at least one test case in TS is statistically significant across repeated executions. The behavioral difference is characterized in terms of the presence of *Miss* objects, *Ghost* objects, and their combination, respectively.

$$isKilled(m, \mathcal{S}) = \begin{cases} \text{True,} & \text{if } \exists img \in TS \text{ such that } \{\mathbb{I}(|\mathcal{S}^{img,i}| > 0)\}_{i=1}^n \text{ is statistically significant,} \\ \text{False,} & \text{otherwise.} \end{cases} \quad (8)$$

where $\mathbb{I}(\cdot)$ is an indicator function that evaluates to 1 if the set is non-empty and 0 otherwise. We employ the one-sample binomial test to determine whether the observed frequency of non-empty sets across n executions is statistically significantly higher than expected by chance. Accordingly, the image-level mutation scores are defined as:

$$Img-MS = \frac{|\{m \in M \mid isKilled(m, \mathcal{S}) = \text{True}\}|}{|M|}, \quad (9)$$

where M is the set of all mutants, $\mathcal{S} \in \{\mathcal{S}_{miss}, \mathcal{S}_{ghost}, \mathcal{S}_{miss} \cup \mathcal{S}_{ghost}\}$, and $isKilled(m, \mathcal{S})$ indicates whether mutant m is killed for the set \mathcal{S} according to the statistical test defined above. Finally, we obtain three image-level mutation scores (MSs): MS_{img}^{miss} , MS_{img}^{ghost} , and MS_{img}^{mg} .

3.3.2 Object-level Mutation Score

Object-level mutation scores evaluate test suite quality by capturing behavioral deviations between the original model and its uncertainty-aware mutants at the level of individual objects. Unlike image-level mutation scores, object-level mutation scores provide a finer-grained view of how predictive uncertainty affects detection outcomes.

We define object-level mutation scores based on the *Miss* and *Ghost* sets, respectively. Specifically, the miss-based object-level mutation score quantifies the proportion of objects that are correctly detected by the original model but are missed by the mutant models:

$$MS_{obj}^{miss} = \frac{|\mathcal{S}_{miss}|}{|\mathcal{S}_{miss}| + |\mathcal{S}_{match}|}, \quad (10)$$

where $|\mathcal{S}_{miss}|$ and $|\mathcal{S}_{match}|$ denote the number of elements in \mathcal{S}_{miss} and \mathcal{S}_{match} , respectively. MS_{obj}^{miss} reflects the sensitivity of a test suite to uncertainty-induced false negatives. Higher values indicate that the test suite more effectively exposes scenarios in which injected uncertainty causes the model to lose previously stable detections.

Similarly, the ghost-based object-level mutation score is defined as:

$$MS_{obj}^{ghost} = \frac{|\mathcal{S}_{ghost}|}{|\mathcal{S}_{miss}| + |\mathcal{S}_{match}| + |\mathcal{S}_{ghost}|}. \quad (11)$$

MS_{obj}^{ghost} measures a test suite's ability to kill mutants by exposing false positives, i.e., objects detected by mutant models but not by the original model. Higher values indicate that the test suite is effective at exposing overconfident or unstable predictions, which is particularly critical in safety-sensitive object detection applications.

Finally, we define the combined object-level mutation score, which accounts for both miss and ghost objects, as:

$$MS_{obj}^{mg} = \frac{|\mathcal{S}_{miss}| + |\mathcal{S}_{ghost}|}{|\mathcal{S}_{miss}| + |\mathcal{S}_{match}| + |\mathcal{S}_{ghost}|}. \quad (12)$$

MS_{obj}^{mg} characterizes overall mutant killability at the object level by jointly considering missed and ghost objects. By capturing both the disappearance of originally detected objects and the emergence of additional detections, it provides a comprehensive measure of behavioral divergence introduced by uncertainty-aware mutations.

3.3.3 IoU-based Mutation Score

IoU-based mutation score evaluates test suite quality by quantifying degradation in spatial overlap for matched objects detected by both the original model and its mutants, which is defined as:

$$MS_{iou} = \frac{1}{|\mathcal{S}_{match}|} \sum_{(d_i, d'_j) \in \mathcal{S}_{match}} (1 - \text{IoU}(b_i, b'_j)), \quad (13)$$

where b_i, b'_j are the bounding boxes corresponding to the detected objects d_i, d'_j from the original model and its mutant, respectively.

3.3.4 Uncertainty-aware Mutation Score

Uncertainty-aware mutation scores evaluate test suite quality by measuring differences in predictive uncertainty between the original model and its mutants. To quantify predictive uncertainty, we execute both the original model and each mutant n times and compute uncertainty metrics from the resulting output distributions. Then, we calculate uncertainty-aware mutation scores for each of the match, miss, and ghost object sets.

Specifically, the uncertainty-aware mutation scores are defined as:

$$UA-MS = |UM_{orig} - UM_{mut}|, \quad (14)$$

where UM_{orig} and UM_{mut} denote the uncertainty metric computed for the original model and the mutant model, respectively, over a given object set. Following Lu et al. [23] (see Section 2.2), we adopt two categories of uncertainty metrics: for classification tasks, we employ VR, SE, and MI; for regression tasks, we employ TV and PS. $UA-MS$ s quantify the extent to which uncertainty-aware mutations affect the model’s predictive uncertainty, thereby reflecting the sensitivity of the test suite to uncertainty-induced behavioral changes. We calculate $UA-MS$ considering each of the three categories of objects (i.e., \mathcal{S}_{match} , \mathcal{S}_{miss} , and \mathcal{S}_{ghost}) and five uncertainty metrics; therefore, we have 15 (3 object sets \times 5 uncertainty metrics) $UA-MS$ s in total.

4 Experiment Design

4.1 Research Questions

In this paper, we plan to answer the following research questions (RQs).

- RQ1: How do the proposed mutation scores compare with the traditional one? RQ1 compares the proposed mutation scores with the traditional ones regarding their effectiveness in differentiating test suite quality under uncertainty.
- RQ2: How well do the proposed mutation scores distinguish test suite quality? RQ2 evaluates the performance of the proposed mutation scores in distinguishing test suites regarding their effectiveness in detecting failures induced by uncertainty. Unlike RQ1, this RQ compares the proposed mutation scores in terms of their ability to differentiate the test suites.
- RQ3: How effective are the proposed MSs in revealing uncertainty in the model? Based on the assumption that higher model uncertainty leads to a higher failure rate, RQ3 investigated the ability of the proposed MSs to detect such degradation under different uncertainty levels.

4.2 Case Studies

We conduct experiments on three industrial case studies: a laptop sticker-removal robot, a laptop disassembling robot, and an entertainment robot. All three robots are equipped with DL-enabled object detection software. The detailed characteristics of each case study are summarized in Table 1.

4.2.1 Laptop Sticker Removing Robot (LSRR)

The Danish Technological Institute (DTI)¹ develops robotic technologies that support a sustainable and circular economy. One of its focuses is robotic systems for refurbishing electronic devices, particularly laptops. To support this goal, an *LSRR* is developed to automate sticker removal from laptop surfaces, a task that is traditionally manual, time-consuming, and prone to inconsistencies. *LSRR* employs a DL-enabled sticker detection software (*STDM*) to localize stickers and estimate their boundaries.

¹<https://www.dti.dk/>

Table 1: Overview of the industrial case studies and experimental configurations, including subject models, test suites, and mutation ratio settings.

Robot	Model	Model Architecture	Test Suite	Mutation Ratio (MCD)	Mutation Ratio (MCB)
<i>TIAGo Pro</i>	<i>HFDM1</i>	<i>YuNet</i>	<i>lowImg, medImg, highImg</i>	0.10	$0.10 \cdot \{1, 3, 5, 7, 9\}$
	<i>HFDM2</i>	<i>YuNet-s</i>		0.15	$0.15 \cdot \{1, 3, 5, 7, 9\}$
<i>LDR</i>	<i>SCDM</i>	<i>YOLOv11</i>	<i>norImg, explm</i>	0.20	$0.20 \cdot \{1, 3, 5, 7, 9\}$
				0.25	$0.25 \cdot \{1, 3, 5, 7, 9\}$
<i>LSRR</i>	<i>STDM1</i>	<i>Faster R-CNN</i>	<i>origImg, dalmg, sdImg</i>	0.30	$0.30 \cdot \{1, 3, 5, 7, 9\}$
	<i>STDM2</i>	<i>Faster R-CNN_v2</i>		0.35	$0.35 \cdot \{1, 3, 5, 7, 9\}$
	<i>STDM3</i>	<i>RetinaNet</i>		0.40	$0.40 \cdot \{1, 3, 5, 7, 9\}$
	<i>STDM4</i>	<i>RetinaNet_v2</i>		0.45	$0.45 \cdot \{1, 3, 5, 7, 9\}$
	<i>STDM5</i>	<i>SSD300</i>		0.50	$0.50 \cdot \{1, 3, 5, 7, 9\}$

Subject DL-enabled Software. We obtain five pre-trained *STDMs* employed in *LSRR* developed by DTI. These *STDMs* are based on various object detection architectures, including *Faster R-CNN* [32], *Faster R-CNN_v2* [33], *RetinaNet* [34], *RetinaNet_v2* [35], *SSD300* [36], and *SSDLite* [37]. They were trained by DTI using a dedicated sticker detection dataset containing thousands of annotated laptop images with stickers in various poses, sizes, and lighting conditions. All five *STDMs* are trained based on the open-source PyTorch implementation [38]. We modify the five *STDMs* to be compatible with the two uncertainty-aware mutation operators by injecting prediction-time-activated dropout/dropblock layers. Specifically, for *Faster R-CNN*, *Faster R-CNN_v2*, *RetinaNet*, and *RetinaNet_v2*, we add dropout/dropblock layers to the last three convolutional layers of the Feature Pyramid Network, a shared component built on top of their backbones. For *SSD300*, we add dropout/dropblock layers to the last three layers of the detection head.

Subject Test Suites. We select three subject test suites: *origImg*, *dalmg*, and *sdImg*. *origImg* contains real-world images collected by DTI, where stickers are manually placed on laptops and annotated by hand. In contrast, *dalmg* and *sdImg* are synthetic test suites generated by prompting two vision-language models to produce realistic laptop images with stickers under diverse conditions. All stickers in *dalmg* and *sdImg* are manually annotated, and each image is manually validated to ensure visual realism. Each test suite contains 150 images and has been used in prior studies as a standardized benchmark [23].

4.2.2 Laptop Disassembling Robot (LDR)

LDR is another robotic system developed by DTI for laptop refurbishment, focusing on automated laptop disassembly. A critical step in the disassembly process is accurate screw localization. To this end, *LDR* integrates DL-enabled screw detection software (*SCDM*) to automatically identify screw positions, which is the foundation for precise and fully automated laptop disassembly.

Subject DL-enabled Software. We obtain one pretrained *SCDM* from DTI, which is based on the *YOLOv11* [39] architecture, and we inject prediction-time-activated dropout/dropblock layers into the last three convolutional layers of the *YOLOv11* backbone.

Subject Test Suites. We obtain two test suites from DTI, i.e., *norImg* and *explm*, each consisting of images of laptops with screws. *norImg* contains 25 images captured under standard lighting conditions representative of typical operating environments, while *explm* contains 125 images captured under varying exposure levels, including both underexposed and overexposed conditions. Both test suites are manually annotated, providing ground-truth labels for screws and their corresponding screw holders.

4.2.3 TIAGo Pro

PAL Robotics² is a leading robotic manufacturer in Spain, with deployments across diverse domains, including warehouses, retail spaces, healthcare, and offices. Notably, *TIAGo Pro* is an open-source mobile manipulator designed for advanced research and applied development. It integrates autonomous navigation, dexterous manipulation, and multimodal perception within a unified platform, featuring a mobile base, a torque-controlled robotic arm, and configurable end-effectors. To operate in dynamic environments, *TIAGo Pro* incorporates RGB-D cameras, LiDAR, and force-torque sensing, and supports various perception and decision-making modules for tasks such as object detection and human-robot interaction. Specifically, *TIAGo Pro* employs DL-enabled human face detection software (*HFDM*) to support its face detection and recognition.

²<https://pal-robotics.com/>

Subject DL-enabled Software. We use two pretrained *HFDMs* in *TIAGo Pro*, both based on the *YuNet* architecture [40]. *YuNet* is a lightweight face detector capable of millisecond-level inference, making it suitable for real-time applications. It is widely applied in embedded systems, mobile devices, and robotic platforms, where efficient and accurate face detection is critical for responsive human-robot interaction. The two *HFDMs* include the standard *YuNet* and a smaller variant, *YuNet-s*, optimized for faster inference. Similarly, to enable the prediction-time dropout/dropblock, we modify the last three convolutional layers of the common backbones of *YuNet* and *YuNet-s*.

Subject Test Suites. According to PAL, the *HFDMs* are pretrained on public data, and no dedicated test suites were specifically collected for evaluation. Therefore, we adopt WIDER FACE [41], the largest publicly available face detection dataset, to construct the subject test suites. Concretely, we select the test set of WIDER FACE and partition it into three subsets based on the number of objects per image, using the 25% (1), 50% (3), and 75% (9) percentiles as thresholds. These subsets are denoted as *lowImg*, *medImg*, and *highImg*, corresponding to images with low, medium, and high object densities, respectively. Specifically, *lowImg* contains 1416 images with 1 to 3 objects, *medImg* contains 309 images with 4 to 9 objects, and *highImg* contains 88 images with 10 or more objects.

4.3 Mutation Ratio

Recall from Section 3.2 that the mutation ratio controls the extent of uncertainty injected by the mutation operators. In our experiments, we configure the mutation operators with multiple mutation ratios to generate diverse mutants. Table 1 summarizes the detailed configurations of the mutation ratios. For the *MCD* operator, we use nine dropout rates ranging from 0.10 to 0.50 in increments of 0.05 as the mutation ratios. For the *MCB* operator, we consider all combinations of these nine dropout rates with five block sizes {1,3,5,7,9}, yielding a total of 45 configurations. The generated mutants are evaluated across all relevant test suites in each case study. These mutation ratios are chosen to systematically explore the models’ sensitivity to different levels and patterns of predictive uncertainty, and have also been adopted in prior works [21, 23, 27].

4.4 Evaluation Metrics

Table 2 presents the metrics used to answer each research question (RQ). Since RQ1 focuses on comparing the proposed mutation scores with the traditional mutation score, we use the image-level mutation score (*Img-MS*) as the baseline metric for comparison with the three types of proposed mutation scores (i.e., *Obj-MS*, *IoU-MS*, and *UA-MS*). RQ2 and RQ3 focus on evaluating test suite quality using the new metrics and investigating the impact of uncertainty on the mutation scores; therefore, we employ *Obj-MS*, *IoU-MS*, and *UA-MS* to perform this analysis.

Table 2: Description of tasks, employed case studies, metrics, and statistical tests for each RQ.

RQs	Tasks (Section 4.1)	Case Study (Section 4.2)	Metrics (Section 4.4)	Statistical Tests (Section 4.5)
RQ1	Compare the proposed MSs with traditional MSs	<i>TIAGo Pro</i> , <i>LDR</i> , <i>LSRR</i>	<i>Img-MS</i> (baseline metrics), <i>Obj-MS</i> , <i>IoU-MS</i> , <i>UA-MS</i>	/
RQ2	Evaluate how effectively the proposed MSs distinguish the quality of different test suites		<i>Obj-MS</i> , <i>IoU-MS</i> , <i>UA-MS</i>	Kruskal–Wallis test, Eta-squared (η^2) effect size
RQ3	Examine how mutant behavior changes under different levels of predictive uncertainty			Spearman’s correlation test Multiple Correlation Coefficient (<i>R</i>), F-test

4.5 Statistical Tests

To answer RQ2, we employ the Kruskal-Wallis rank test [42] at a significance level of 0.01 to determine if there are significant differences among all paired groups (test suites), with a *p-value* < 0.01 indicating a significant difference. We then calculate eta-squared (η^2) as the effect size, ranging from 0 to 1. Following commonly used thresholds [43], η^2 values of $0.01 \leq \eta^2 < 0.06$ indicate a small effect, $0.06 \leq \eta^2 < 0.14$ indicate a moderate effect, and $\eta^2 \geq 0.14$ indicate a large effect. In RQ3, we study the correlation between mutation ratios and mutation scores to see how the change of uncertainty affects the performance of mutation scores. Therefore, we perform the Spearman’s rank correlation (ρ) test [44], a non-parametric test that measures the monotonic relationship between two ranked variables. Values of $\rho \in (0, 1]$ indicate a positive correlation, $\rho \in [-1, 0)$ shows a negative correlation, 1.0 (-1.0) indicates a perfect positive (negative) correlation, and 0 means no correlation. Correlation is considered statistically significant if *p-value* < 0.01. Following Mukaka [45], we divide ρ into five levels: *negligible* ($\rho \in (-0.300, 0.300)$), *low* ($\rho \in [0.300, 0.500)$ or $(-0.500, -0.300]$), *moderate* ($\rho \in [0.50, 0.700)$ or $(-0.700, 0.500]$), *high* ($\rho \in [0.700, 0.900)$ or $(-0.900,$

-0.700]), and *very high* ($\rho \in [0.900, 1.000]$ or $[-1.000, -0.900]$). Recall that *MCB* operator has two mutation ratios (dropout rate and block size) that together control the mutation of a model; therefore, for *MCB*, we employ the multiple correlation coefficient (R) [46] to measure the effect of the combined mutation ratios on mutation scores. F-test is applied to assess the statistical significance of the multiple correlation test, with p -value < 0.01 indicating a significant correlation. Following Hinkle et al. [47], R is interpreted using five levels: *negligible* ($R \in [0, 0.300)$), *low* ($R \in [0.300, 0.500)$), *moderate* ($R \in [0.50, 0.700)$), *high* ($R \in [0.700, 0.900)$), and *very high* ($R \in [0.900, 1.000]$).

5 Results and Analysis

5.1 Results for RQ1 – Proposed vs. Traditional Mutation Scores

Table 3 and Table 4 present the descriptive results of mutation scores achieved by each test suite across different case studies. For the *TIAGo Pro* case study, which has two subject models (*HFDM1* and *HFDM2*) and three subject test suites (*lowImg*, *medImg*, and *highImg*), all three *Img-MS* metrics (MS_{img}^{miss} , MS_{img}^{ghost} , and MS_{img}^{mg}) do not differentiate among the test suites. In contrast, the three *Obj-MS* and the *IoU-MS* metrics exhibit a clear and consistent decreasing trend from *lowImg* to *highImg* for both models, differentiating the three test suites (TSs). Similarly, the *UA-MS* metrics largely follow this pattern: 11 out of the 15 *UA-MS* metrics demonstrate a clear decreasing trend from *lowImg* to *medImg* and further to *highImg*, indicating that test suites with fewer objects are more effective at revealing uncertainty-induced failures.

Table 3: Mutation Scores Achieved by Different Test Suites on *HFDM1*, *HFDM2*, *SCDM1*, and *STDM1* – RQ1.

Metrics	<i>HFDM1</i>			<i>HFDM2</i>			<i>SCDM1</i>		<i>STDM1</i>			
	<i>lowImg</i>	<i>medImg</i>	<i>highImg</i>	<i>lowImg</i>	<i>medImg</i>	<i>highImg</i>	<i>norImg</i>	<i>explng</i>	<i>origImg</i>	<i>dalng</i>	<i>sdImg</i>	
<i>Img-MS</i>	MS_{img}^{miss}	1.000	1.000	1.000	1.000	1.000	1.000	0.000	1.000	0.481	1.000	1.000
	MS_{img}^{ghost}	1.000	1.000	1.000	1.000	1.000	1.000	0.204	0.796	1.000	1.000	1.000
	MS_{img}^{mg}	1.000	1.000	1.000	1.000	1.000	1.000	0.204	1.000	1.000	1.000	1.000
<i>Obj-MS</i>	MS_{obj}^{miss}	0.499	0.320	0.192	0.482	0.273	0.165	0.000	0.006	0.000	0.015	0.025
	MS_{obj}^{ghost}	0.346	0.270	0.175	0.461	0.337	0.217	0.000	0.002	0.009	0.014	0.019
	MS_{obj}^{mg}	0.662	0.496	0.327	0.708	0.507	0.336	0.000	0.008	0.010	0.028	0.043
<i>IoU-MS</i>	MS_{iou}	0.580	0.419	0.304	0.563	0.378	0.270	0.034	0.048	0.049	0.065	0.072
<i>UA-MS</i>	MS_{vr}^{match}	0.476	0.317	0.208	0.462	0.278	0.180	0.000	0.006	0.000	0.015	0.023
	MS_{ie}^{match}	0.362	0.239	0.152	0.356	0.210	0.130	0.003	0.014	0.007	0.020	0.026
	MS_{mi}^{match}	0.476	0.309	0.194	0.461	0.270	0.169	0.000	0.007	0.001	0.018	0.028
	MS_{va}^{match}	0.974	0.963	0.929	0.966	0.951	0.899	0.410	0.407	0.900	0.969	0.972
	MS_{ps}^{match}	0.957	0.971	0.975	0.958	0.973	0.975	0.911	0.910	0.984	0.991	0.992
	MS_{vr}^{miss}	0.606	0.539	0.528	0.593	0.507	0.496	0.000	0.015	0.001	0.063	0.071
	MS_{ie}^{miss}	0.469	0.418	0.415	0.460	0.394	0.386	0.000	0.014	0.001	0.036	0.040
	MS_{mi}^{miss}	0.606	0.539	0.528	0.593	0.507	0.496	0.000	0.015	0.001	0.063	0.071
	MS_{va}^{miss}	0.606	0.539	0.528	0.593	0.507	0.496	0.000	0.015	0.001	0.063	0.071
	MS_{ps}^{miss}	0.606	0.539	0.528	0.593	0.507	0.496	0.000	0.015	0.001	0.063	0.071
	MS_{vr}^{ghost}	0.154	0.153	0.146	0.152	0.152	0.147	0.001	0.005	0.020	0.046	0.060
	MS_{ie}^{ghost}	0.101	0.101	0.099	0.100	0.100	0.099	0.001	0.005	0.007	0.016	0.020
	MS_{mi}^{ghost}	0.152	0.152	0.145	0.151	0.151	0.147	0.001	0.005	0.019	0.044	0.058
	MS_{va}^{ghost}	0.076	0.077	0.080	0.081	0.082	0.083	0.001	0.004	0.007	0.013	0.015
	MS_{ps}^{ghost}	0.102	0.103	0.104	0.102	0.102	0.103	0.001	0.004	0.010	0.020	0.027

In terms of the *LDR* case study, which has one subject model (*STDM1*) and two test suites (*norImg* and *explng*), all *Img-MS*, *Obj-MS*, and *IoU-MS* metrics show clear differences between the two test suites, and 13 out of 15 *UA-MS* yield a higher quality of *explng* than *norImg*, suggesting that *explng* is more effective in exposing uncertainty-related failures for *STDM1*.

The *LSRR* case study has five subject models (*STDM1* – *STDM5*) and three test suites (*origImg*, *dalng*, and *sdImg*). For *STDM1*, the MS_{img}^{miss} metric indicates that *origImg* has the worst quality, but cannot distinguish between *dalng* and *sdImg*. For MS_{img}^{ghost} and MS_{img}^{mg} , they remain consistently the same across all three test suites, indicating limited distinguishing ability. In contrast, the *Obj-MS* and *IoU-MS* metrics exhibit an increasing trend from *origImg* to *dalng* and further to *sdImg*, indicating that these metrics are more sensitive in differentiating test suites. Similarly, all *UA-MS*

Table 4: Mutation Scores Achieved by Different Test Suites on *STDM2*, *STDM3*, *STDM4*, *STDM5* – RQ1.

Metrics	STDM2			STDM3			STDM4			STDM5			
	<i>origImg</i>	<i>dalng</i>	<i>sdImg</i>	<i>origImg</i>	<i>dalng</i>	<i>sdImg</i>	<i>origImg</i>	<i>dalng</i>	<i>sdImg</i>	<i>origImg</i>	<i>dalng</i>	<i>sdImg</i>	
<i>Img-MS</i>	MS_{img}^{miss}	0.593	1.000	1.000	1.000	1.000	1.000	0.981	0.778	1.000	1.000	1.000	1.000
	MS_{img}^{ghost}	0.889	1.000	1.000	1.000	1.000	1.000	1.000	1.000	1.000	1.000	1.000	1.000
	MS_{img}^{mg}	0.907	1.000	1.000	1.000	1.000	1.000	1.000	1.000	1.000	1.000	1.000	1.000
<i>Obj-MS</i>	MS_{obj}^{miss}	0.002	0.029	0.037	0.010	0.009	0.022	0.005	0.006	0.025	0.274	0.049	0.049
	MS_{obj}^{ghost}	0.004	0.012	0.032	0.006	0.012	0.006	0.002	0.005	0.010	0.523	0.474	0.490
	MS_{obj}^{mg}	0.005	0.041	0.067	0.015	0.021	0.027	0.007	0.011	0.035	0.635	0.500	0.515
<i>Obj-MS</i>	MS_{iou}	0.044	0.067	0.070	0.044	0.042	0.052	0.034	0.029	0.047	0.389	0.262	0.272
<i>UA-MS</i>	MS_{vr}^{match}	0.002	0.027	0.031	0.010	0.008	0.021	0.005	0.006	0.027	0.181	0.049	0.049
	MS_{ie}^{match}	0.020	0.043	0.048	0.020	0.021	0.032	0.009	0.015	0.025	0.211	0.098	0.089
	MS_{mi}^{match}	0.005	0.035	0.039	0.013	0.012	0.025	0.005	0.009	0.027	0.202	0.073	0.069
	MS_{va}^{match}	0.889	0.967	0.971	0.838	0.941	0.952	0.744	0.815	0.778	0.949	0.999	0.999
	MS_{ps}^{match}	0.983	0.985	0.991	0.979	0.984	0.989	0.966	0.942	0.911	0.948	0.998	0.998
	MS_{vr}^{miss}	0.004	0.089	0.098	0.026	0.023	0.062	0.013	0.013	0.070	0.345	0.088	0.097
	MS_{ie}^{miss}	0.004	0.053	0.067	0.026	0.022	0.054	0.013	0.012	0.054	0.305	0.079	0.086
	MS_{mi}^{miss}	0.004	0.089	0.098	0.026	0.023	0.062	0.013	0.013	0.070	0.345	0.088	0.097
	MS_{va}^{miss}	0.004	0.089	0.098	0.026	0.023	0.062	0.013	0.013	0.070	0.345	0.088	0.097
	MS_{ps}^{miss}	0.004	0.089	0.098	0.026	0.023	0.062	0.013	0.013	0.070	0.345	0.088	0.097
	MS_{vr}^{ghost}	0.011	0.036	0.094	0.015	0.048	0.023	0.005	0.013	0.037	0.199	0.214	0.216
	MS_{ie}^{ghost}	0.005	0.016	0.029	0.007	0.041	0.022	0.003	0.012	0.026	0.133	0.133	0.135
	MS_{mi}^{ghost}	0.011	0.034	0.089	0.016	0.048	0.023	0.005	0.013	0.036	0.192	0.205	0.207
	MS_{va}^{ghost}	0.006	0.014	0.019	0.006	0.010	0.012	0.002	0.006	0.008	0.060	0.056	0.056
	MS_{ps}^{ghost}	0.009	0.021	0.031	0.007	0.014	0.018	0.003	0.007	0.011	0.110	0.107	0.107

metrics consistently reveal improved quality from *origImg*, *dalng*, to *sdImg*. This pattern extends to the remaining models (*STDM2*–*STDM5*), where *Img-MS* metrics remain identical across all test suites in 8 out of 12 cases, whereas *Obj-MS*, *IoU-MS*, and *UA-MS* consistently reveal differences in test suites. Overall, these results indicate that proposed mutation scores (*Obj-MS*, *IoU-MS*, and *UA-MS*) are consistently more effective than *Img-MS* in distinguishing the quality of different test suites.

Conclusion for RQ1: Compared to the traditional mutation score (*Img-MS*), the novel mutation scores (*Obj-MS*, *IoU-MS*, and *UA-MS*) are more effective at distinguishing test suite quality in revealing uncertainty-induced failures in DL-enabled software across six out of seven models in three case studies. This indicates that the proposed mutation score metrics provide a more sensitive and reliable assessment of test suite quality than traditional ones in the presence of uncertainty.

5.2 Results for RQ2 – Effectiveness in Distinguishing Test Suites

To answer RQ2, we apply the non-parametric Kruskal–Wallis test to compute *p-values*, assessing whether statistically significant differences exist among test suites. We also calculate eta-squared (η^2) to quantify the effect size. The results are shown in Table 5. For *Obj-MS* metrics, MS_{obj}^{miss} and MS_{obj}^{mg} achieve statistically significant results on all models ($p < 0.01$), indicating their strong performance in distinguishing test suite quality. Notably, MS_{obj}^{miss} consistently achieves a large effect size ($\eta^2 \geq 0.14$) across all models, whereas MS_{obj}^{mg} shows large effect sizes for the majority but moderate effect sizes for *STDM3* and *STDM5*. The performance of MS_{obj}^{ghost} is also strong with significant differences and large effect sizes for most models, except for *STDM5*, where the difference is not statistically significant ($p = 0.271$). Similarly, the *IoU-MS* metric can significantly distinguish between different test suites for all models, and the effect sizes vary from large magnitudes for *HFDM2* ($\eta^2 = 0.712$) to moderate for *SCDM1* ($\eta^2 = 0.132$) and small for *STDM3* ($\eta^2 = 0.054$).

Regarding the *UA-MS* metrics, the ability to distinguish test suite quality varies across metrics. When looking at *UA-MS* calculated based on the match set (\mathcal{S}_{match}), MS_{vr}^{match} , MS_{ie}^{match} , and MS_{mi}^{match} demonstrate consistently significant differences among different test suites with large effect sizes across nearly all models, indicating that these metrics are highly effective at distinguishing test suite quality. MS_{va}^{match} and MS_{ps}^{match} also demonstrate significant

Table 5: **Statistical Results Using the Kruskal–Wallis Test and Eta-Squared Effect Size – RQ2.** A bold η^2 with $p < 0.01$ indicates a statistically significant difference. The η^2 effect sizes are further interpreted as: **Large** if $\eta^2 \geq 0.14$, **Moderate** if $0.06 \leq \eta^2 < 0.14$, and **Small** if $0.01 \leq \eta^2 < 0.06$.

Metrics	HFDM1		HFDM2		SCDM1		STDM1		STDM2		STDM3		STDM4		STDM5		
	p	η^2	p	η^2	p	η^2	p	η^2	p	η^2	p	η^2	p	η^2	p	η^2	
Obj-MS	MS_{obj}^{miss}	<0.01	0.604	<0.01	0.692	<0.01	0.856	<0.01	0.747	<0.01	0.653	<0.01	0.385	<0.01	0.565	<0.01	0.571
	MS_{obj}^{ghost}	<0.01	0.433	<0.01	0.384	<0.01	0.276	<0.01	0.236	<0.01	0.730	<0.01	0.370	<0.01	0.664	0.271	0.004
	MS_{obj}^{mg}	<0.01	0.545	<0.01	0.544	<0.01	0.717	<0.01	0.612	<0.01	0.703	<0.01	0.113	<0.01	0.625	<0.01	0.106
IoU-MS	MS_{iou}	<0.01	0.639	<0.01	0.712	<0.01	0.132	<0.01	0.185	<0.01	0.310	<0.01	0.054	<0.01	0.212	<0.01	0.294
UA-MS	MS_{vr}^{match}	<0.01	0.559	<0.01	0.642	<0.01	0.856	<0.01	0.746	<0.01	0.639	<0.01	0.439	<0.01	0.596	<0.01	0.551
	MS_{ie}^{match}	<0.01	0.703	<0.01	0.769	<0.01	0.516	<0.01	0.421	<0.01	0.252	<0.01	0.136	<0.01	0.348	<0.01	0.423
	MS_{mi}^{match}	<0.01	0.625	<0.01	0.694	<0.01	0.743	<0.01	0.747	<0.01	0.572	<0.01	0.332	<0.01	0.568	<0.01	0.513
	MS_{va}^{match}	<0.01	0.572	<0.01	0.588	0.902	0.000	<0.01	0.473	<0.01	0.538	<0.01	0.486	<0.01	0.145	<0.01	0.651
	MS_{ps}^{match}	<0.01	0.226	<0.01	0.307	0.888	0.000	<0.01	0.430	<0.01	0.545	<0.01	0.402	<0.01	0.855	<0.01	0.626
	MS_{vr}^{miss}	<0.01	0.107	<0.01	0.203	<0.01	0.857	<0.01	0.673	<0.01	0.661	<0.01	0.383	<0.01	0.600	<0.01	0.557
	MS_{ie}^{miss}	<0.01	0.123	<0.01	0.247	<0.01	0.856	<0.01	0.670	<0.01	0.638	<0.01	0.362	<0.01	0.578	<0.01	0.534
	MS_{mi}^{miss}	<0.01	0.107	<0.01	0.203	<0.01	0.856	<0.01	0.673	<0.01	0.661	<0.01	0.383	<0.01	0.600	<0.01	0.557
	MS_{va}^{miss}	<0.01	0.107	<0.01	0.203	<0.01	0.857	<0.01	0.673	<0.01	0.661	<0.01	0.383	<0.01	0.600	<0.01	0.557
	MS_{ps}^{miss}	<0.01	0.107	<0.01	0.203	<0.01	0.857	<0.01	0.673	<0.01	0.661	<0.01	0.383	<0.01	0.600	<0.01	0.557
	MS_{vr}^{ghost}	<0.01	0.050	0.040	0.028	<0.01	0.266	<0.01	0.521	<0.01	0.785	<0.01	0.509	<0.01	0.783	0.020	0.036
	MS_{ie}^{ghost}	0.340	0.001	0.400	0.000	<0.01	0.330	<0.01	0.415	<0.01	0.696	<0.01	0.653	<0.01	0.804	0.536	0.000
	MS_{mi}^{ghost}	<0.01	0.047	0.048	0.026	<0.01	0.266	<0.01	0.525	<0.01	0.787	<0.01	0.494	<0.01	0.774	0.029	0.032
	MS_{va}^{ghost}	<0.01	0.087	0.183	0.009	<0.01	0.236	<0.01	0.257	<0.01	0.428	<0.01	0.193	<0.01	0.484	<0.01	0.056
	MS_{ps}^{ghost}	<0.01	0.177	<0.01	0.171	<0.01	0.251	<0.01	0.330	<0.01	0.500	<0.01	0.268	<0.01	0.347	<0.01	0.095

differences among different test suites with large effect sizes on six out of seven models, with one exception observed for *SCDM1*, where the results are not statistically significant ($p > 0.01$). For *UA-MS* metrics calculated based on S_{miss} set (MS_{vr}^{miss} , MS_{ie}^{miss} , MS_{mi}^{miss} , MS_{va}^{miss} , and MS_{ps}^{miss}), a stable pattern is observed where all metrics consistently yield statistically significant differences among different test suites across all models; the effect sizes are large for six out of seven models, with *HFDM1* exhibiting moderate magnitudes. Finally, the performance of the ghost set (S_{ghost}) based *UA-MS* metrics varies across models. MS_{vr}^{ghost} , MS_{ie}^{ghost} , MS_{mi}^{ghost} , and MS_{va}^{ghost} are highly effective at distinguishing test suites for *SCDM1* and *STDM1*–*STDM4*, with significant differences and large effect sizes observed; however, for *HFDM1*, *HFDM2*, and *STDM5*, these metrics exhibit non-significant or significant but small effect sizes. One possible explanation for this discrepancy is that the mutants associated with models such as *HFDM* detect fewer ghost objects. Consequently, the limited number of detected ghost objects results in lower variance within these metrics, reducing their ability to distinguish between test suites. Notably, MS_{ps}^{ghost} demonstrates statistically significant differences among different test suites for all models, with effect sizes ranging from moderate to large.

Conclusion for RQ2: The proposed mutation scores are effective in distinguishing the test suite’s ability to reveal uncertainty-induced failures in DL-enabled software. In particular, *IoU-MS* and *Obj-MS* (especially MS_{obj}^{miss} and MS_{obj}^{mg}) consistently demonstrate statistically significant differences in test suites across all models. Among *UA-MS*, MS_{vr}^{match} , MS_{ie}^{match} , MS_{mi}^{match} , all *UA-MS* derived from S_{miss} , and MS_{ps}^{ghost} are the most stable and effective in highlighting differences between test suites, indicating their sensitivity to uncertainty-induced failures.

5.3 Results for RQ3 – Effect of Uncertainty on Mutation Scores

To answer RQ3, we first visualize the trends of each mutation score as the mutation ratio varies, and then conduct correlation tests to analyze the correlation between the mutation ratios and mutation scores. Given that multiple test suites are employed for each model, we merge the mutation score data across all test suites to obtain comprehensive results for all test suites. We then analyze the mutation score results separately for each mutation operator: the *MCD* and *MCB* operators, as introduced in Section 3.2.

5.3.1 Analysis for *MCD* Operator

Recall from Section 3.2 that *MCD* operator generates mutants of a given model using the MC-Dropout method [20], and it has one mutation ratio called dropout rate to control the probability of neurons being dropped during inference time. A higher dropout rate indicates greater uncertainty injected into the model. Figs. 3 and 4 present the results for *MCD* operator, showing the mean MS values and their 95% confidence interval (CI) across different dropout rates

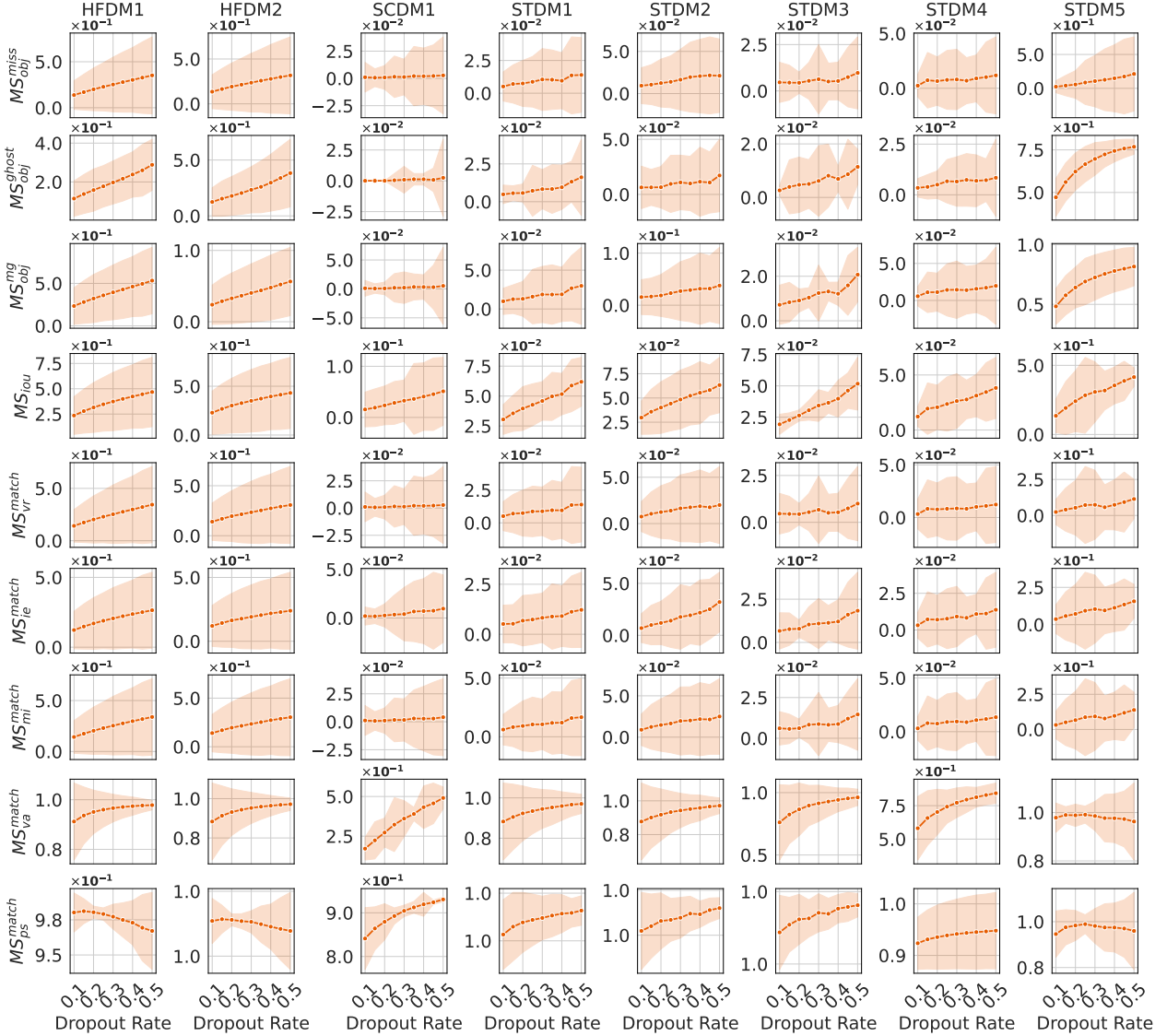


Figure 3: Mutation Scores Achieved by Test Suites with 95% Confidence Intervals for Different Dropout Rates (Mutation Operator: *MCD*, Mutation Scores: *Obj-MS*, *IoU-MS*, and *UA-MS* derived from \mathcal{S}_{match}) – RQ3.

for each model. Table 6 further reports the correlation test results between dropout rate and all mutation scores using Spearman’s rank correlation test.

Descriptive Statistics. As Figs. 3 and 4 show, in general, as the dropout rate increases, the values increase across the majority of mutation score metrics and models. This pattern aligns with the expectation that a higher dropout rate induces greater uncertainty, thereby inducing a higher frequency of failures in the generated mutants. Consequently, the increase in mutation scores indicates that most of them effectively capture uncertainty-induced degradation in model behavior. Furthermore, the 95% CI regions generally grow as the dropout rate increases, indicating higher variability in mutation score values. This suggests that while the mutation scores are sensitive to changes in model uncertainty, higher levels of uncertainty may reduce their stability.

When looking at each metric, different patterns are observed for specific mutation score metrics, which is interesting for further analysis. First, all *Obj-MS* and *IoU-MS* metrics demonstrate a consistent increasing trend across all models as the dropout rate increases. This confirms their general effectiveness in detecting model performance degradation caused by the increase in model uncertainty. However, this sensitivity comes at the cost of stability, as widening CIs is observed at higher dropout rates. A similar pattern is observed for MS_{vr}^{match} , MS_{ie}^{match} , MS_{mi}^{match} , and all *UA-MS* metrics derived from \mathcal{S}_{miss} . Their values consistently increase across all models as the dropout rate increases, while

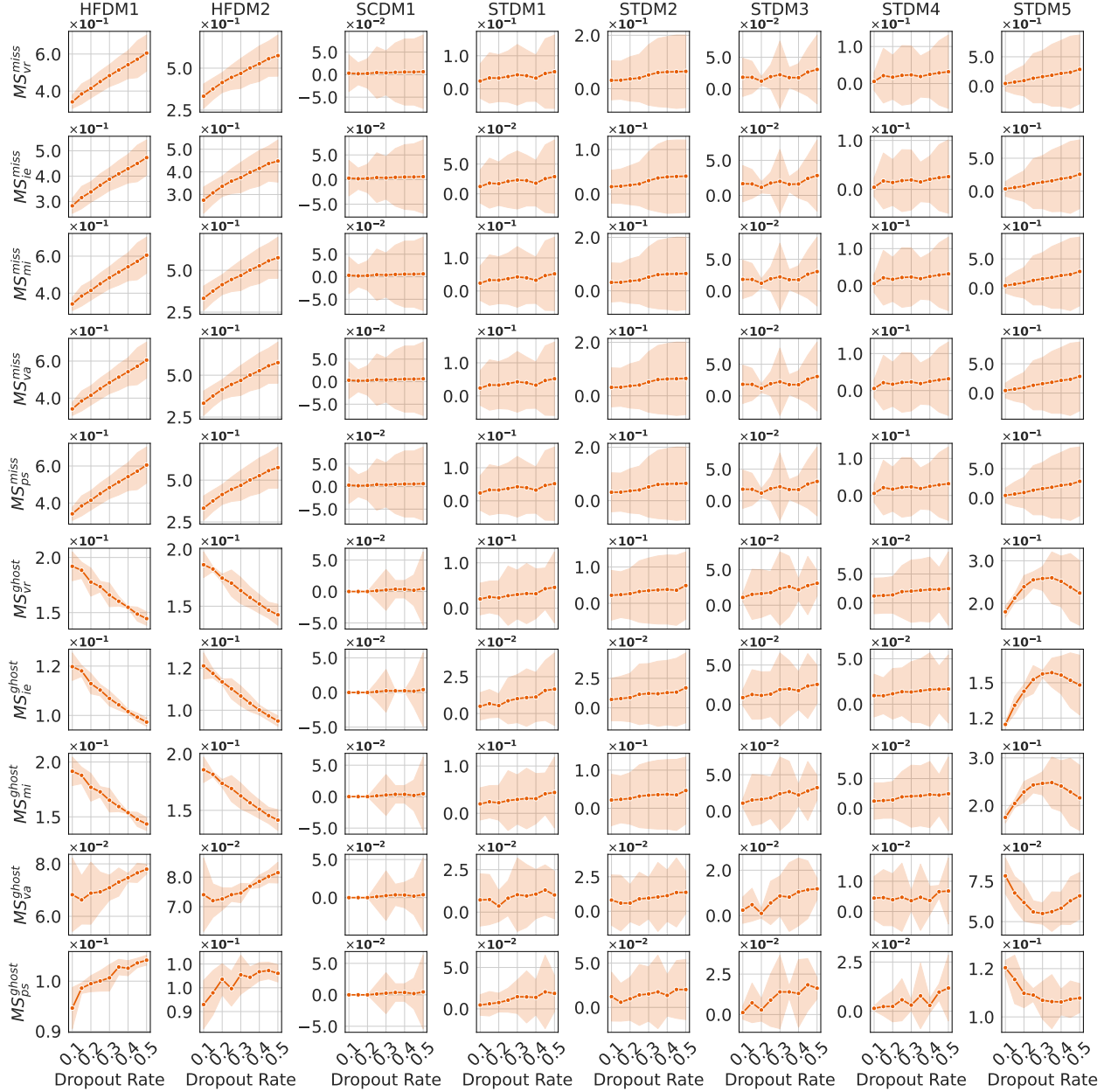


Figure 4: Mutation Scores Achieved by Test Suites with 95% Confidence Intervals for Different Dropout Rates (Mutation Operator: *MCD*, Mutation Scores: *UA-MS* Derived from \mathcal{S}_{miss} and \mathcal{S}_{ghost}) – RQ3.

exhibiting higher variances. This indicates that these *UA-MS* metrics are capable of capturing uncertainty-induced model performance degradation.

However, notable exceptions are observed for MS_{va}^{match} , MS_{ps}^{match} , and all *UA-MS* derived from \mathcal{S}_{ghost} . Although MS_{va}^{match} and MS_{ps}^{match} increase in certain cases (e.g., *STDM1* and *STDM1* to *STDM4*), they exhibit a flat or even negative trend for models such as *HFDM1* and *HFDM2*. Interestingly, their CIs become narrower as the dropout rate increases, indicating improved stability as the uncertainty increases. Given that MS_{va}^{match} and MS_{ps}^{match} quantify uncertainty-aware mutation scores in regression outputs (i.e., bounding box coordinates), these results indicate that these two metrics are not effective in capturing the model quality degradation. By inspecting the detection results, we notice a reduction in the size of the match set as the dropout rate increases. A plausible explanation is that increased uncertainty causes the model to entirely miss objects that are hard to detect (shifting them to the miss set); consequently, the objects remaining in the match set are easy targets where the model maintains confident regression predictions, leading to low

or stable values in MS_{va}^{match} and MS_{ps}^{match} even as overall model performance degrades. As for $UA-MS$ derived from S_{ghost} , they exhibit different patterns for different models. Specifically, MS_{vr}^{ghost} , MS_{ie}^{ghost} , and MS_{mi}^{ghost} show the expected positive increase trend for $SCDM1$ and $STDM1$ to $STDM4$. However, for $HFDM1$, $HFDM2$, and $STDM5$, they either exhibit negative correlations or no clear trend. This model-specific pattern is likely attributed to the number and characteristics of ghost objects generated by each model.

Correlation Analysis. As Table 6 shows, $Obj-MS$ and $IoU-MS$ metrics exhibit a statistically significant and very high positive correlation ($\rho \approx 1.000$) with the dropout rate across nearly all models. This statistically confirms that increasing the dropout rate (corresponding to greater uncertainty), consistently leads to higher mutation score values. This observation confirms that these metrics are effective in capturing the model degradation under varying uncertainty levels.

Table 6: **Correlation Test Results between Dropout Rates and Mutation Scores for MC-Dropout-based Mutation Operator Using Spearman’s Rank Correlation (ρ) test – RQ3.** Bold values indicate statistically significant correlations ($p < 0.01$). The ρ values are further interpreted as: **Very High** if $\rho \in [0.900, 1.000]$ or $[-1.000, -0.900]$, **High** if $\rho \in [0.700, 0.900]$ or $[-0.900, -0.700]$, **Moderate** if $\rho \in [0.50, 0.700]$ or $[-0.700, 0.500]$, and **Low** if $\rho \in [0.300, 0.500]$ or $[-0.500, -0.300]$.

Metrics		HFDM1		HFDM2		SCDM1		STDM1		STDM2		STDM3		STDM4		STDM5	
		p	ρ	p	ρ	p	ρ	p	ρ	p	ρ	p	ρ	p	ρ	p	ρ
Obj-MS	MS_{obj}^{miss}	<0.01	1.000	<0.01	1.000	<0.01	0.917	<0.01	0.933	<0.01	0.983	<0.01	0.800	<0.01	0.867	<0.01	1.000
	MS_{obj}^{ghost}	<0.01	1.000	<0.01	1.000	<0.01	0.877	<0.01	1.000	<0.01	0.917	<0.01	0.983	<0.01	0.933	<0.01	1.000
	MS_{obj}^{ps}	<0.01	1.000	<0.01	1.000	<0.01	0.883	<0.01	0.983	<0.01	1.000	<0.01	0.950	<0.01	0.950	<0.01	1.000
IoU-MS	MS_{iou}	<0.01	1.000	<0.01	1.000	<0.01	1.000	<0.01	1.000	<0.01	1.000	<0.01	1.000	<0.01	1.000	<0.01	1.000
	MS_{vr}^{match}	<0.01	1.000	<0.01	1.000	<0.01	0.917	<0.01	0.983	<0.01	0.983	<0.01	0.800	<0.01	0.933	<0.01	0.917
	MS_{ie}^{match}	<0.01	1.000	<0.01	1.000	<0.01	0.983	<0.01	1.000	<0.01	1.000	<0.01	1.000	<0.01	0.967	<0.01	0.983
	MS_{mi}^{match}	<0.01	1.000	<0.01	1.000	<0.01	0.883	<0.01	1.000	<0.01	0.983	<0.01	0.933	<0.01	0.933	<0.01	0.950
	MS_{va}^{match}	<0.01	1.000	<0.01	1.000	<0.01	1.000	<0.01	1.000	<0.01	1.000	<0.01	1.000	<0.01	1.000	0.013	-0.783
	MS_{ps}^{match}	<0.01	-0.950	<0.01	-0.950	<0.01	1.000	<0.01	1.000	<0.01	0.983	<0.01	0.983	<0.01	1.000	0.460	-0.283
UA-MS	MS_{vr}^{miss}	<0.01	1.000	<0.01	1.000	<0.01	0.929	0.030	0.717	<0.01	1.000	0.224	0.450	<0.01	0.867	<0.01	1.000
	MS_{ie}^{miss}	<0.01	1.000	<0.01	1.000	<0.01	0.933	0.013	0.783	<0.01	1.000	0.205	0.467	<0.01	0.867	<0.01	1.000
	MS_{mi}^{miss}	<0.01	1.000	<0.01	1.000	<0.01	0.933	0.030	0.717	<0.01	1.000	0.224	0.450	<0.01	0.867	<0.01	1.000
	MS_{va}^{miss}	<0.01	1.000	<0.01	1.000	<0.01	0.929	0.030	0.717	<0.01	1.000	0.224	0.450	<0.01	0.867	<0.01	1.000
	MS_{ps}^{miss}	<0.01	1.000	<0.01	1.000	<0.01	0.929	0.030	0.717	<0.01	1.000	0.224	0.450	<0.01	0.867	<0.01	1.000
	MS_{vr}^{ghost}	<0.01	-1.000	<0.01	-1.000	<0.01	0.877	<0.01	0.967	<0.01	0.950	<0.01	0.950	<0.01	0.983	0.433	0.300
	MS_{ie}^{ghost}	<0.01	-1.000	<0.01	-1.000	<0.01	0.865	<0.01	0.983	<0.01	0.983	<0.01	0.933	<0.01	0.967	0.139	0.533
	MS_{mi}^{ghost}	<0.01	-1.000	<0.01	-1.000	<0.01	0.865	<0.01	0.967	<0.01	0.950	<0.01	0.950	<0.01	0.983	0.308	0.383
	MS_{va}^{ghost}	<0.01	0.983	<0.01	0.950	<0.01	0.865	<0.01	0.817	<0.01	0.950	<0.01	0.933	0.205	0.467	0.516	-0.250
	MS_{ps}^{ghost}	<0.01	0.983	<0.01	0.917	<0.01	0.877	<0.01	0.917	<0.01	0.833	<0.01	0.900	<0.01	0.883	0.025	-0.733

The correlation results for $UA-MS$ reveal different patterns for specific metrics. For $UA-MS$ derived from S_{match} , MS_{vr}^{match} , MS_{ie}^{match} , MS_{mi}^{match} , and MS_{va}^{match} exhibit statistically significant and very high positive correlations across nearly all models. A notable exception is MS_{ps}^{match} for $HFDM1$ and $HFDM2$, which shows a strong negative correlation ($\rho = -0.950$), and this aligns with the prior observation from Figure 3 and 4. For the $UA-MS$ derived from S_{miss} , statistically significant and high or very high positive correlations are observed for the majority of models (e.g., $HFDM1$, $HFDM2$, $SCDM1$, and $STDM2$, 4, 5). This indicates that these metrics are effective in capturing the increased uncertainty-induced failures, particularly those related to missed detections. However, $STDM1$ and $STDM3$ exhibit a deviation where the correlations are not statistically significant ($p > 0.05$), indicating limited effectiveness in capturing model failures as the increase of uncertainty for these two specific models. Finally, the Ghost set metrics highlight the most significant architectural disparities under varying uncertainty levels. While $SCDM1$ and most $STDM$ models show positive correlations, $HFDM1$ and $HFDM2$ exhibit a perfect negative correlation ($\rho = -1.000$) for MS_{vr}^{ghost} , MS_{ie}^{ghost} , and MS_{mi}^{ghost} . Interestingly, this trend reverses for MS_{va}^{ghost} and MS_{ps}^{ghost} in the same $HFDM$ models, where the correlation is strongly positive. Recall that MS_{vr}^{ghost} , MS_{ie}^{ghost} , and MS_{mi}^{ghost} are derived from classification uncertainty, whereas MS_{va}^{ghost} and MS_{ps}^{ghost} are derived from regression uncertainty. This indicates that as overall model uncertainty increases, the classification predictions of ghost objects remain relatively stable, while the bounding box predictions become more unstable.

5.3.2 Analysis for MCB Operator

MCB operator generates mutants of a given model using the MC-DropBlock method [21]. Unlike the MCD operator, which is governed by a single mutation ratio, MCB operator employs two mutation ratios: the dropout rate determining

the proportion of activations perturbed, and the block size, controlling the spatial granularity of the injected uncertainty. Higher mutation ratios indicate a greater injected uncertainty. Figs. 5 and 6 present the results for the *MCB* operator, illustrating how each mutation score varies across different combinations of dropout rate and block size for each model. Table 6 further reports the multiple correlation results between mutation scores and the combinations of dropout rate and block size.

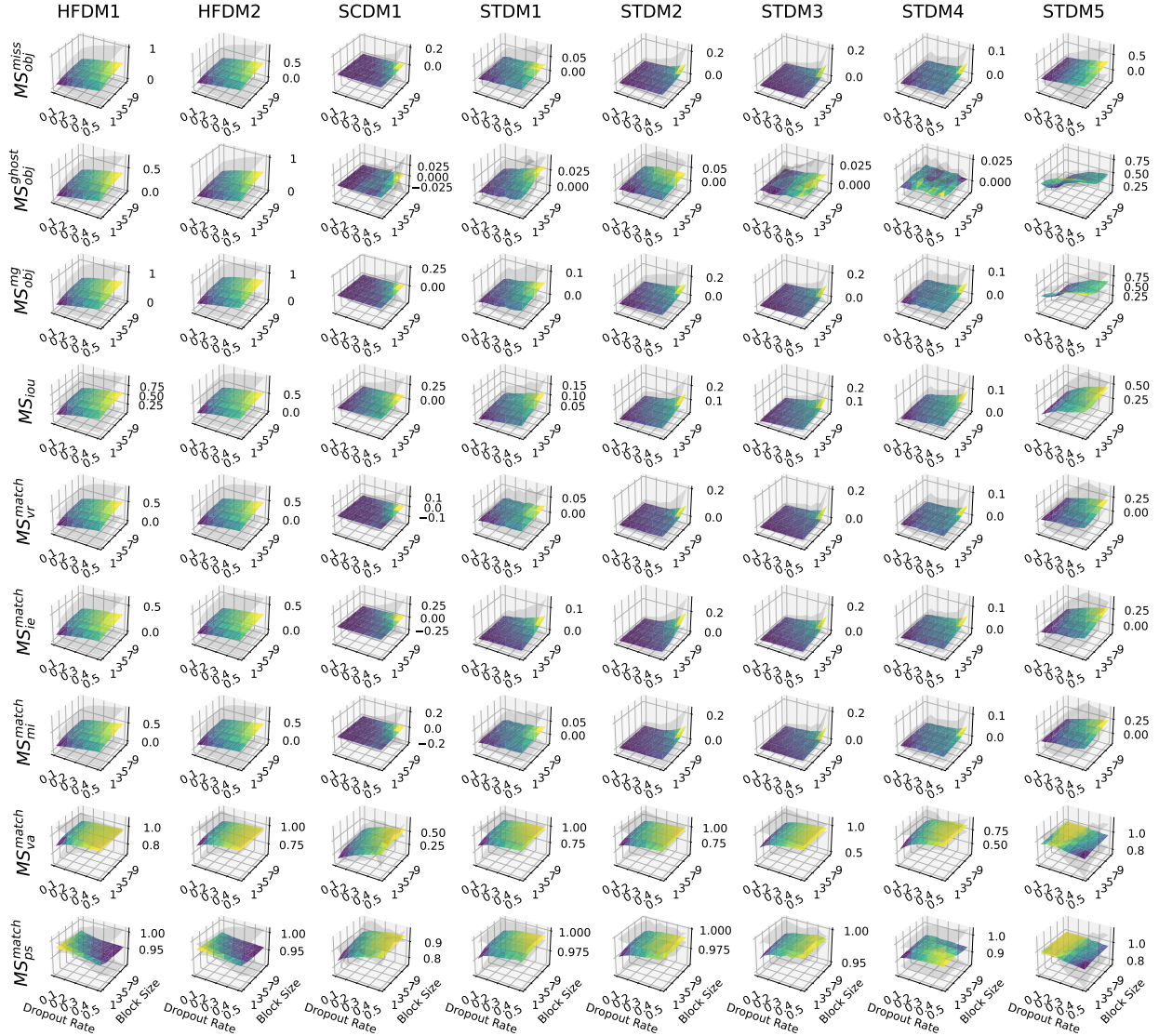


Figure 5: Mutation Scores Achieved by Test Suites with 95% Confidence Intervals for Dropout Rates \times Block Sizes (Mutation Operator: *MCB*, Mutation Scores: *Obj-MS*, *IoU-MS*, and *UA-MS* derived from \mathcal{S}_{match}) – RQ3.

Descriptive Statistics. As shown in Figs. 5 and 6, mutation scores generally increase with both dropout rate and block size, indicating their effectiveness in capturing uncertainty-induced degradation in model performance. Besides, among the two mutation ratios, block size appears to have a greater impact than dropout rate, often leading to steeper gradients in mutation score surfaces. At the level of individual metric, both *Obj-MS* and *IoU-MS* metrics exhibit clear monotonic gradients, with surfaces sloping upward toward regions corresponding to larger block sizes and higher dropout rates. This behavior highlights the effectiveness and sensitivity of *Obj-MS* and *IoU-MS* metrics in capturing uncertainty-induced failures under varying uncertainty levels.

Similarly, *UA-MS* demonstrates consistent upward trends across MS_{vr}^{match} , MS_{ie}^{match} , MS_{mi}^{match} , MS_{va}^{match} , as well as across all *UA-MS* metrics derived from \mathcal{S}_{miss} , confirming that these metrics reliably capture model uncertainty. However, for MS_{ps}^{match} , and all *UA-MS* derived from \mathcal{S}_{ghost} , the surfaces exhibit flatter patterns and no distinct

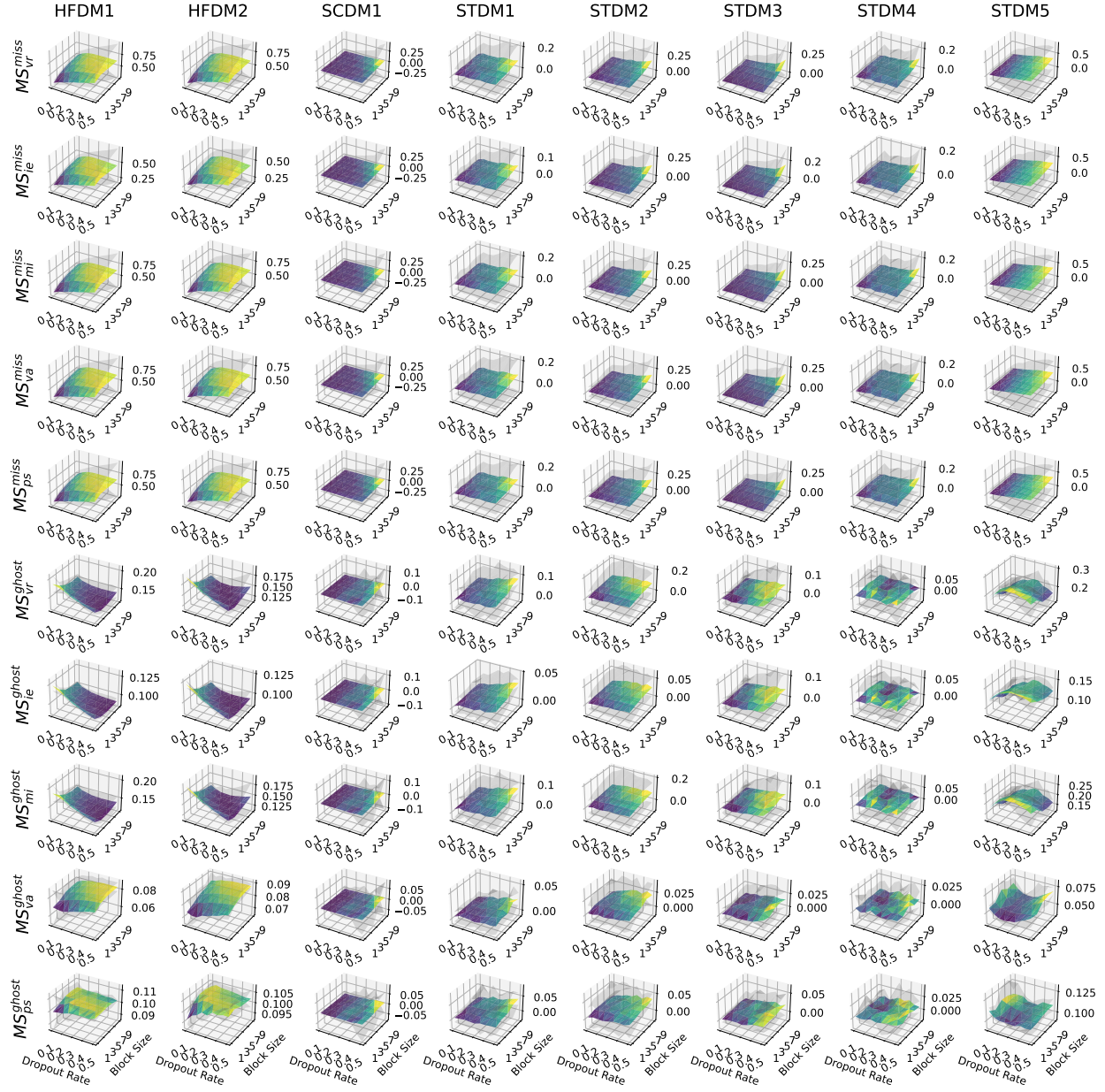


Figure 6: Mutation Scores Achieved by Test Suites with 95% Confidence Intervals for Dropout Rates \times Block Sizes (Mutation Operator: *MCB*, Mutation Scores: *UA-MS* Derived from \mathcal{S}_{miss} and \mathcal{S}_{ghost}) – RQ3.

monotonic gradients are observed. This behavior suggests that these metrics are less effective in capturing the model’s performance degradation as uncertainty increases. A possible reason might relate to the detection nature of the ghost and miss objects, that ghost objects act as false positives driven by random noise; their internal uncertainty estimates tend to be irregular and do not scale linearly with the mutation ratios.

Multiple Correlation Analysis. Table 7 shows the results of the multiple correlation analysis between mutation scores and the combination of dropout rate and block size. The analysis reveals that the majority of the correlations are statistically significant ($p < 0.01$) and range from high to very high correlation, confirming that the proposed mutation scores are effective metrics capable of capturing uncertainty-induced performance degradation. Specifically, the *Obj-MS* and the *IoU-MS* exhibit the strongest correlation with the combined two mutation ratios. For instance, MS_{iou} consistently achieves very high correlation coefficients ($R > 0.90$) across nearly all case studies, such as $R = 0.987$ for *SCDM1* and $R = 0.977$ for *STDM5*. Similarly, the *Obj-MS* maintain high correlation values in most cases, e.g., 0.985

Table 7: **Multiple Correlation Test Results between (Dropout Rate, Block Size) and Mutation Scores for MCB Operator Using Multiple Correlation Coefficient (R) – RQ3.** Bold values indicate statistically significant correlations ($p < 0.01$). The R values are further interpreted as: **Very High** if $R \in [0.900, 1.000]$, **High** if $R \in [0.700, 0.900]$, **Moderate** if $R \in [0.50, 0.700]$, and **Low** if $R \in [0.300, 0.500]$.

Metrics		HFDM1		HFDM2		SCDM1		STDM1		STDM2		STDM3		STDM4		STDM5	
		p	R														
Obj-MS	MS_{obj}^{miss}	<0.01	0.974	<0.01	0.976	<0.01	0.814	<0.01	0.951	<0.01	0.805	<0.01	0.751	<0.01	0.829	<0.01	0.984
	MS_{obj}^{ghost}	<0.01	0.976	<0.01	0.985	<0.01	0.856	<0.01	0.952	<0.01	0.966	<0.01	0.898	0.013	0.432	<0.01	0.917
	MS_{obj}^{mb}	<0.01	0.969	<0.01	0.979	<0.01	0.846	<0.01	0.966	<0.01	0.903	<0.01	0.800	<0.01	0.849	<0.01	0.924
IoU-MS	MS_{iou}	<0.01	0.957	<0.01	0.968	<0.01	0.987	<0.01	0.977	<0.01	0.915	<0.01	0.898	<0.01	0.951	<0.01	0.977
UA-MS	MS_{vr}^{match}	<0.01	0.970	<0.01	0.975	<0.01	0.792	<0.01	0.930	<0.01	0.764	<0.01	0.736	<0.01	0.834	<0.01	0.947
	MS_{ie}^{match}	<0.01	0.947	<0.01	0.960	<0.01	0.883	<0.01	0.897	<0.01	0.837	<0.01	0.851	<0.01	0.909	<0.01	0.967
	MS_{mi}^{match}	<0.01	0.967	<0.01	0.973	<0.01	0.827	<0.01	0.949	<0.01	0.802	<0.01	0.778	<0.01	0.862	<0.01	0.958
	MS_{va}^{match}	<0.01	0.810	<0.01	0.882	<0.01	0.961	<0.01	0.917	<0.01	0.923	<0.01	0.927	<0.01	0.902	<0.01	0.767
	MS_{ps}^{match}	<0.01	0.935	<0.01	0.940	<0.01	0.925	<0.01	0.925	<0.01	0.910	<0.01	0.913	<0.01	0.518	<0.01	0.916
	MS_{vr}^{miss}	<0.01	0.861	<0.01	0.860	<0.01	0.831	<0.01	0.927	<0.01	0.909	<0.01	0.825	<0.01	0.848	<0.01	0.990
	MS_{ie}^{miss}	<0.01	0.798	<0.01	0.786	<0.01	0.826	<0.01	0.929	<0.01	0.869	<0.01	0.819	<0.01	0.843	<0.01	0.990
	MS_{mi}^{miss}	<0.01	0.861	<0.01	0.860	<0.01	0.831	<0.01	0.927	<0.01	0.909	<0.01	0.825	<0.01	0.848	<0.01	0.990
	MS_{va}^{miss}	<0.01	0.861	<0.01	0.860	<0.01	0.831	<0.01	0.927	<0.01	0.909	<0.01	0.825	<0.01	0.848	<0.01	0.990
	MS_{ps}^{miss}	<0.01	0.861	<0.01	0.860	<0.01	0.831	<0.01	0.927	<0.01	0.909	<0.01	0.825	<0.01	0.848	<0.01	0.990
	MS_{vr}^{ghost}	<0.01	0.831	<0.01	0.743	<0.01	0.848	<0.01	0.932	<0.01	0.963	<0.01	0.887	0.037	0.381	<0.01	0.656
	MS_{ie}^{ghost}	<0.01	0.881	<0.01	0.849	<0.01	0.863	<0.01	0.950	<0.01	0.962	<0.01	0.896	0.084	0.334	<0.01	0.718
	MS_{mi}^{ghost}	<0.01	0.833	<0.01	0.747	<0.01	0.848	<0.01	0.934	<0.01	0.963	<0.01	0.887	0.045	0.371	<0.01	0.653
	MS_{va}^{ghost}	<0.01	0.908	<0.01	0.937	<0.01	0.810	<0.01	0.854	<0.01	0.903	<0.01	0.787	0.021	0.410	<0.01	0.545
	MS_{ps}^{ghost}	0.118	0.311	0.052	0.363	<0.01	0.839	<0.01	0.910	<0.01	0.900	<0.01	0.814	<0.01	0.572	<0.01	0.495

for MS_{obj}^{ghost} in HFDM2. This observation confirms the earlier conclusion that these metrics have clear monotonic gradients and are highly sensitive to the uncertainty in the models. As for UA-MS metrics, the metrics derived match and miss sets achieve significant and moderate to very high correlations with the mutation ratios, indicating their effectiveness in capturing the uncertainty-induced failures in the models. However, the correlation strengths for UA-MS metrics derived from the ghost set are notably weaker, particularly regarding the MS_{ps}^{ghost} . As the table shows, for HFDM1 and HFDM2, the correlation between MS_{ps}^{ghost} and the combined mutation ratios is statistically insignificant ($p > 0.05$), while for STDM5, the correlation is low ($R = 0.495$), indicating limited sensitivity of these metrics to uncertainty-induced faults in ghost objects. Furthermore, STDM4 exhibits insignificant correlations across four of the five ghost-related UA-MS metrics. These findings are consistent with our previous findings and validate the flat surface phenomenon observed in the descriptive analysis, indicating that the UA-MS derived from the ghost set are irregular and do not scale linearly with the models' uncertainty.

Conclusion for RQ3: The proposed mutation scores are generally effective in capturing uncertainty-induced failures of DL-enabled software, and are sensitive to varying uncertainty levels. Among all mutation scores, *Obj-MS* and *IoU-MS* metrics are the most effective, showing consistently high to very high correlation with the mutation ratios across both *MCD* and *MCB* operators, though higher uncertainty can affect their stability. Furthermore, the UA-MS derived from the match set are the most stable metrics for *MCD* operator, while the UA-MS derived from the match and miss sets are the most stable metrics for *MCB* operator.

5.4 Data Availability

To enable the reproducibility of our findings, we provide the replication package in our GitHub online repository³. The replication package contains the following contents: 1) the related algorithms and source code for experimenting; 2) the data and code for the experiment results and analysis.

6 Discussion

Incorporating Uncertainty in Mutation Analysis. In traditional mutation analysis for DL-enabled software, mutants are designed to simulate faults in DL models; however, they often fail to capture the stochastic behavior inherent in DL models. To address this limitation, we propose uncertainty-aware mutation operators that explicitly model

³<https://github.com/Simula-COMPLEX/UAMTERS>

uncertainty in DL models. Consequently, uncertainty-aware mutation analysis provides a more faithful representation of potential failures that self-adaptive robotic systems may encounter under unpredictable, dynamic conditions, enabling a systematic evaluation of test suite effectiveness in revealing uncertainty-induced model degradation. Moreover, we introduce uncertainty-aware mutation scores to quantify a test suite’s effectiveness in exposing failures induced by stochastic perturbations. Compared to traditional mutation scores, these scores provide a more fine-grained assessment of test suite quality and can further guide the development of tests that enhance safety, reliability, and performance under real-world operating conditions.

Supporting Uncertainty-Aware Mutation Testing. While *UAMTERS* primarily focuses on mutation analysis of test suites, it can support the mutation testing of DL-enabled software. Mutation testing relies on the premise that test suites with high mutation scores are more likely to expose faults in the original program, whereas low mutation scores indicate less effective test suites and therefore highlight the need for improvement. Under this premise, uncertainty-aware mutation testing provides a systematic way to identify high-quality test suites and guide the improvement of low-quality ones that fail to expose uncertainty-induced degradation. Specifically, after evaluating test suite quality via mutation analysis, uncertainty-aware mutation testing can refine or augment low-quality test suites, e.g., by introducing adversarial perturbations [48], to construct new test suites that more effectively reveal uncertainty-induced degradation. This iterative process enables continuous improvement of test suites that can effectively evaluate the model behaviors under uncertainty. Developing such uncertainty-aware mutation testing techniques is our future work.

Supporting the MAPLE-K Loop for Self-Adaptive Robots. *UAMTERS* directly supports the Legitimate component of the MAPLE-K loop for self-adaptive robots. It enables the systematic evaluation of test suites in exposing uncertainty-induced failures, allowing test suites generated by various test generation approaches to be effectively compared. By leveraging these insights, the Legitimate component can make more informed decisions about whether planned adaptations satisfy safety and performance requirements before execution, thereby enhancing the trustworthiness and reliability of self-adaptive robots in real-world operation. In addition, the novel mutation scores can further guide and improve test generation. For instance, they can be used to define the objective functions that guide the generation of more effective test suites. Another potential application is to support test prioritization, ensuring that higher quality tests are executed first to efficiently detect potential failures. Beyond the Legitimate component, *UAMTERS* can also support other components of the MAPLE-K loop. For example, the Knowledge component can store model uncertainty and test suite quality information, enriching the system’s historical knowledge for future decision-making. Similarly, insights from *UAMTERS* could inform the Analyze component by highlighting uncertainty-related failure patterns, and guide the Plan component to generate more robust adaptation strategies.

7 Threats to Validity

Conclusion Validity relates to the validity and reliability of the conclusions. To draw reliable conclusions, we first adopt the statistical definition of mutation killing proposed by Jahangirova and Tonella [9], which accounts for the stochastic nature of DL models. In addition, we employ appropriate statistical tests and conduct rigorous analysis in accordance with established guidelines.

Construct Validity concerns the definition of mutation scores. The scores are defined based on the well-established performance metrics and uncertainty metrics, e.g., IoU and Entropy, commonly used in evaluating DL-based systems. This ensures that the mutation scores reflect test suite effectiveness in revealing performance degradation under uncertainty.

Internal Validity concerns the parameter settings. To determine the mutation ratios for the mutation operators, we follow the dropout rate settings from Lu et al. [23] and the block size settings from Yelleni et al. [21] to select the mutation ratios. Besides, the selection of network layers to which the Dropout or DropBlock layers are applied may influence the observed mutation effects. To reduce this threat, we follow common practice in uncertainty quantification [27, 23] by applying the mutation operators to the last three convolutional layers.

External Validity is about the generalizability of this study. First, the selection of the subject robotic systems can potentially threaten the external validity. To mitigate this threat, we select three industrial-level robotic systems comprising seven DL-enabled object detection software and eight test suites representative of real-world, safety-critical applications. Second, we admit that the mutation scores are designed for object detection tasks, which may limit their direct applicability to other DL tasks or model architectures. Nevertheless, focusing on object detection remains essential, as it’s a core perception task in robots, supporting safety-critical functions such as navigation, obstacle avoidance, and human–robot interaction. Dedicated mutation scores, therefore, enable a more accurate evaluation of test suite effectiveness in revealing uncertainty-induced degradation. Besides, while these metrics are designed for object detection models, the underlying uncertainty-aware mutation testing methodology is general and can be adapted to other DL tasks.

8 Related Work

Mutation analysis is a widely applied technique for evaluating test suite quality for software systems and can support a range of activities, including test generation [49, 50], test prioritization [51], and fault localization [52, 53]. In recent years, mutation analysis has been extended to DL, with specialized mutation operators developed to simulate realistic faults in neural networks. These operators can target various aspects of DL models, including weights, neuron activations, layer connections, and input data [54, 6, 55]. For example, MuNN [54] is a mutation analysis tool which integrates five mutation operators covering both domain-dependent and depth-dependent mutations for DL. DeepMutation [6] proposes to inject faults into DL models using both source-level and model-level mutation operators. Later, DeepMutation++ [7] extended DeepMutation by introducing mutation operators specifically tailored for recurrent neural networks. Jahangirova and Tonella [9] conduct an empirical evaluation to identify effective mutation operators and introduce a statistical definition of mutation killing. To simulate real DL faults, Humbačová et al. [8] propose DeepCrime, which integrates 35 mutation operators by analyzing existing real DL faults. Although DeepCrime includes a mutation operator that modifies dropout layers, it is designed as a regularization operator applied during training and does not explicitly model predictive uncertainty or systematically assess uncertainty-induced behavioral changes. In contrast, our dropout-based operator is designed as an uncertainty-aware mutation operator applied at prediction time, enabling the explicit modeling and evaluation of predictive uncertainty.

Moreover, mutation analysis has been applied to guide mutation testing. For example, Tambon et al. [56] introduce PMT, a probabilistic mutation testing approach that accounts for stochastic model behavior to provide more consistent and reliable mutation-based test evaluations in DL models. Wang et al. [57] employ mutation analysis to prioritize test inputs for DL models, improving the effectiveness of test suites in revealing model weaknesses. Dang et al. [58] propose GraphPrior, a mutation-based approach for graph neural networks that ranks test inputs by the number of mutated models they kill, improving fault detection on both natural and adversarial inputs. Wang et al. [59] propose a runtime detection method for adversarial examples based on mutation testing, demonstrating that adversarial inputs exhibit higher sensitivity to model mutations than normal inputs. Pour et al. [48] propose a search-based testing framework for DL in source code embedding tasks, where mutation testing is used to guide adversarial test generation.

While these works have advanced mutation analysis and testing for DL, they do not explicitly address failures related to model uncertainty, which is crucial in safety-critical applications such as robotics [23] and autonomous driving [60]. In this paper, we specifically focus on model failures that are related to model uncertainty and propose two uncertainty-aware mutation operators to inject uncertainty into the models. In addition, we design 19 novel mutation scores that capture different perspectives of model behavior, enabling a more comprehensive assessment of test suite effectiveness in detecting uncertainty-related performance degradation.

9 Conclusion

To evaluate test suite quality, we present *UAMTERS*, an uncertainty-aware mutation analysis framework for DL-enabled software in robots. *UAMTERS* introduces novel mutation operators that explicitly inject stochastic uncertainty into DL models, enabling the systematic simulation of uncertainty-induced behaviors. In addition, we define novel uncertainty-aware mutation scores to quantify a test suite’s ability to reveal model degradation and behavioral changes under varying levels of uncertainty. The empirical evaluation on three industrial-level robotic case studies demonstrates that *UAMTERS* more effectively distinguishes test suite quality and captures uncertainty-induced failures compared to traditional mutation scores. By explicitly considering uncertainty, *UAMTERS* provides a more informative evaluation of test suite effectiveness, supporting the validation of dependability in self-adaptive robots. In the future, we plan to extend *UAMTERS* by integrating additional uncertainty-aware mutation operators and metrics designed for more complex DL models, including vision language action models. We also aim to investigate strategies for integrating *UAMTERS* into continuous testing pipelines for self-adaptive robots, enabling real-time assessment of test suite quality under evolving operational conditions. Furthermore, studying the impact of different types of uncertainty on test effectiveness could provide deeper insights into designing robust and resilient robots.

Acknowledgments

This work is supported by the RoboSAPIENS project funded by the European Commission’s Horizon Europe programme (No. 101133807). Jiahui Wu is also supported by the Co-tester (No. 314544) project funded by the Research Council of Norway.

References

- [1] Martin Zimmermann and Franz Wotawa. An adaptive system for autonomous driving. *Software Quality Journal*, 28(3):1189–1212, 2020.
- [2] Danny Weyns, Ilias Gerostathopoulos, Nadeem Abbas, Jesper Andersson, Stefan Biffi, Premek Brada, Tomas Bures, Amleto Di Salle, Matthias Galster, Patricia Lago, Grace Lewis, Marin Litoiu, Angelika Musil, Juergen Musil, Panos Patros, and Patrizio Pelliccione. Self-adaptation in industry: A survey. *ACM Trans. Auton. Adapt. Syst.*, 18(2), May 2023.
- [3] Tongtong Wang, Robert Skulstad, and Houxiang Zhang. Physics-informed neural networks for robust system identification of ship roll dynamics with noise resilience. *IEEE Transactions on Industrial Informatics*, 2025.
- [4] Yarin Gal et al. Uncertainty in deep learning. 2016.
- [5] Artúr István Károly, Péter Galambos, József Kuti, and Imre J Rudas. Deep learning in robotics: Survey on model structures and training strategies. *IEEE Transactions on Systems, Man, and Cybernetics: Systems*, 51(1):266–279, 2020.
- [6] Lei Ma, Fuyuan Zhang, Jiyuan Sun, Minhui Xue, Bo Li, Felix Juefei-Xu, Chao Xie, Li Li, Yang Liu, Jianjun Zhao, et al. Deepmutation: Mutation testing of deep learning systems. In *2018 IEEE 29th international symposium on software reliability engineering (ISSRE)*, pages 100–111. IEEE, 2018.
- [7] Qiang Hu, Lei Ma, Xiaofei Xie, Bing Yu, Yang Liu, and Jianjun Zhao. Deepmutation++: A mutation testing framework for deep learning systems. In *2019 34th IEEE/ACM International Conference on Automated Software Engineering (ASE)*, pages 1158–1161. IEEE, 2019.
- [8] Nargiz Humbatova, Gunel Jahangirova, and Paolo Tonella. Deepcrime: mutation testing of deep learning systems based on real faults. In *Proceedings of the 30th ACM SIGSOFT international symposium on software testing and analysis*, pages 67–78, 2021.
- [9] Gunel Jahangirova and Paolo Tonella. An empirical evaluation of mutation operators for deep learning systems. In *2020 IEEE 13th International Conference on Software Testing, Validation and Verification (ICST)*, pages 74–84. IEEE, 2020.
- [10] Peter G Larsen, Shaukat Ali, Roland Behrens, Ana Cavalcanti, Claudio Gomes, Guoyuan Li, Paul De Meulenaere, Mikkel L Olsen, Nikolaos Passalis, Thomas Peyrucain, et al. Robotic safe adaptation in unprecedented situations: the robosapiens project. *Research Directions: Cyber-Physical Systems*, 2:e4, 2024.
- [11] Paolo Arcaini, Elvinia Riccobene, and Patrizia Scandurra. Modeling and analyzing mape-k feedback loops for self-adaptation. In *2015 IEEE/ACM 10th International Symposium on Software Engineering for Adaptive and Self-Managing Systems*, pages 13–23. IEEE, 2015.
- [12] Karoline Nylænder, Aitor Arrieta, Shaukat Ali, and Paolo Arcaini. Search-based generation of waypoints for triggering self-adaptations in maritime autonomous vessels. In *Proceedings of the Genetic and Evolutionary Computation Conference, GECCO '25*, page 1453–1461, New York, NY, USA, 2025. Association for Computing Machinery.
- [13] Athanasios Voulodimos, Nikolaos Doulamis, Anastasios Doulamis, and Eftychios Protopapadakis. Deep learning for computer vision: A brief review. *Computational intelligence and neuroscience*, 2018(1):7068349, 2018.
- [14] Daniel W. Otter, Julian R. Medina, and Jugal K. Kalita. A survey of the usages of deep learning for natural language processing. *IEEE Transactions on Neural Networks and Learning Systems*, 32(2):604–624, 2021.
- [15] Mohsen Soori, Behrooz Arezoo, and Roza Dastres. Artificial intelligence, machine learning and deep learning in advanced robotics, a review. *Cognitive Robotics*, 3:54–70, 2023.
- [16] Jakob Gawlikowski, Cedrique Rovile Njjeutcheu Tassi, Mohsin Ali, Jongseok Lee, Matthias Humt, Jianxiang Feng, Anna Kruspe, Rudolph Triebel, Peter Jung, Ribana Roscher, et al. A survey of uncertainty in deep neural networks. *Artificial Intelligence Review*, 56(Suppl 1):1513–1589, 2023.
- [17] Xiyue Zhang, Xiaofei Xie, Lei Ma, Xiaoning Du, Qiang Hu, Yang Liu, Jianjun Zhao, and Meng Sun. Towards characterizing adversarial defects of deep learning software from the lens of uncertainty. In *Proceedings of the ACM/IEEE 42nd International Conference on Software Engineering, ICSE '20*, page 739–751, New York, NY, USA, 2020. Association for Computing Machinery.
- [18] Michael Weiss and Paolo Tonella. Fail-safe execution of deep learning based systems through uncertainty monitoring. In *2021 14th IEEE Conference on Software Testing, Verification and Validation (ICST)*, pages 24–35, 2021.

- [19] Dustin Tran, Mike Dusenberry, Mark Van Der Wilk, and Danijar Hafner. Bayesian layers: A module for neural network uncertainty. *Advances in neural information processing systems*, 32, 2019.
- [20] Yarin Gal and Zoubin Ghahramani. Dropout as a bayesian approximation: Representing model uncertainty in deep learning. In *international conference on machine learning*, pages 1050–1059. PMLR, 2016.
- [21] Sai Harsha Yelleni, Deepshikha Kumari, et al. Monte carlo dropblock for modeling uncertainty in object detection. *Pattern Recognition*, 146:110003, 2024.
- [22] Balaji Lakshminarayanan, Alexander Pritzel, and Charles Blundell. Simple and scalable predictive uncertainty estimation using deep ensembles. *Advances in neural information processing systems*, 30, 2017.
- [23] Chengjie Lu, Jiahui Wu, Shaikat Ali, and Mikkel Labori Olsen. Assessing the uncertainty and robustness of the laptop refurbishing software. In *2025 IEEE Conference on Software Testing, Verification and Validation (ICST)*, pages 406–416. IEEE, 2025.
- [24] Linton C Freeman. Elementary applied statistics: for students in behavioral science. (*No Title*), 1965.
- [25] Claude Elwood Shannon. A mathematical theory of communication. *The Bell system technical journal*, 27(3):379–423, 1948.
- [26] Di Feng, Lars Rosenbaum, and Klaus Dietmayer. Towards safe autonomous driving: Capture uncertainty in the deep neural network for lidar 3d vehicle detection. In *2018 21st international conference on intelligent transportation systems (ITSC)*, pages 3266–3273. IEEE, 2018.
- [27] Ferhat Ozgur Catak, Tao Yue, and Shaikat Ali. Prediction surface uncertainty quantification in object detection models for autonomous driving. In *2021 IEEE international conference on artificial intelligence testing (AITest)*, pages 93–100. IEEE, 2021.
- [28] Alexander D’Amour, Katherine Heller, Dan Moldovan, Ben Adlam, Babak Alipanahi, Alex Beutel, Christina Chen, Jonathan Deaton, Jacob Eisenstein, Matthew D Hoffman, et al. Underspecification presents challenges for credibility in modern machine learning. *Journal of Machine Learning Research*, 23(226):1–61, 2022.
- [29] Xiyue Zhang, Xiaofei Xie, Lei Ma, Xiaoning Du, Qiang Hu, Yang Liu, Jianjun Zhao, and Meng Sun. Towards characterizing adversarial defects of deep learning software from the lens of uncertainty. In *Proceedings of the ACM/IEEE 42nd International Conference on Software Engineering*, pages 739–751, 2020.
- [30] Joseph Redmon, Santosh Divvala, Ross Girshick, and Ali Farhadi. You only look once: Unified, real-time object detection. In *Proceedings of the IEEE conference on computer vision and pattern recognition*, pages 779–788, 2016.
- [31] Haiping Wu, Bin Xiao, Noel Codella, Mengchen Liu, Xiyang Dai, Lu Yuan, and Lei Zhang. Cvt: Introducing convolutions to vision transformers. In *Proceedings of the IEEE/CVF international conference on computer vision*, pages 22–31, 2021.
- [32] Shaoqing Ren, Kaiming He, Ross Girshick, and Jian Sun. Faster r-cnn: Towards real-time object detection with region proposal networks. *Advances in neural information processing systems*, 28, 2015.
- [33] Yanghao Li, Saining Xie, Xinlei Chen, Piotr Dollar, Kaiming He, and Ross Girshick. Benchmarking detection transfer learning with vision transformers. *arXiv preprint arXiv:2111.11429*, 2021.
- [34] Tsung-Yi Lin, Priya Goyal, Ross Girshick, Kaiming He, and Piotr Dollár. Focal loss for dense object detection. In *Proceedings of the IEEE international conference on computer vision*, pages 2980–2988, 2017.
- [35] Shifeng Zhang, Cheng Chi, Yongqiang Yao, Zhen Lei, and Stan Z Li. Bridging the gap between anchor-based and anchor-free detection via adaptive training sample selection. In *Proceedings of the IEEE/CVF conference on computer vision and pattern recognition*, pages 9759–9768, 2020.
- [36] Wei Liu, Dragomir Anguelov, Dumitru Erhan, Christian Szegedy, Scott Reed, Cheng-Yang Fu, and Alexander C Berg. Ssd: Single shot multibox detector. In *Computer Vision—ECCV 2016: 14th European Conference, Amsterdam, The Netherlands, October 11–14, 2016, Proceedings, Part I 14*, pages 21–37. Springer, 2016.
- [37] Andrew Howard, Mark Sandler, Grace Chu, Liang-Chieh Chen, Bo Chen, Mingxing Tan, Weijun Wang, Yukun Zhu, Ruoming Pang, Vijay Vasudevan, et al. Searching for mobilenetv3. In *Proceedings of the IEEE/CVF international conference on computer vision*, pages 1314–1324, 2019.
- [38] Adam Paszke, Sam Gross, Francisco Massa, Adam Lerer, James Bradbury, Gregory Chanan, Trevor Killeen, Zeming Lin, Natalia Gimelshein, Luca Antiga, et al. Pytorch: An imperative style, high-performance deep learning library. *Advances in neural information processing systems*, 32, 2019.
- [39] Rejin Varghese and M Sambath. Yolov8: A novel object detection algorithm with enhanced performance and robustness. In *2024 International conference on advances in data engineering and intelligent computing systems (ADICS)*, pages 1–6. IEEE, 2024.

- [40] Wei Wu, Hanyang Peng, and Shiqi Yu. Yunet: A tiny millisecond-level face detector. *Machine Intelligence Research*, 20(5):656–665, 2023.
- [41] Shuo Yang, Ping Luo, Chen Change Loy, and Xiaoou Tang. Wider face: A face detection benchmark. In *IEEE Conference on Computer Vision and Pattern Recognition (CVPR)*, 2016.
- [42] William H Kruskal and W Allen Wallis. Use of ranks in one-criterion variance analysis. *Journal of the American statistical Association*, 47(260):583–621, 1952.
- [43] Alboukadel Kassambara. *Kruskal-Wallis Effect Size*, 2025. R package version 0.7.3.
- [44] Jerrold H Zar. Spearman rank correlation. *Encyclopedia of biostatistics*, 7, 2005.
- [45] Mavuto M Mukaka. A guide to appropriate use of correlation coefficient in medical research. *Malawi medical journal*, 24(3):69–71, 2012.
- [46] Agustin Garcia Asuero, Ana Sayago, and AG González. The correlation coefficient: An overview. *Critical reviews in analytical chemistry*, 36(1):41–59, 2006.
- [47] Dennis E Hinkle, William Wiersma, Stephen G Jurs, et al. *Applied statistics for the behavioral sciences*, volume 663. Houghton Mifflin Boston, 2003.
- [48] Maryam Vahdat Pour, Zhuo Li, Lei Ma, and Hadi Hemmati. A search-based testing framework for deep neural networks of source code embedding. In *2021 14th IEEE Conference on Software Testing, Verification and Validation (ICST)*, pages 36–46, 2021.
- [49] Hirohide Haga and Akihisa Suehiro. Automatic test case generation based on genetic algorithm and mutation analysis. In *2012 IEEE International Conference on Control System, Computing and Engineering*, pages 119–123. IEEE, 2012.
- [50] Richard Baker and Ibrahim Habli. An empirical evaluation of mutation testing for improving the test quality of safety-critical software. *IEEE Transactions on Software Engineering*, 39(6):787–805, 2012.
- [51] Donghwan Shin, Shin Yoo, Mike Papadakis, and Doo-Hwan Bae. Empirical evaluation of mutation-based test case prioritization techniques. *Software Testing, Verification and Reliability*, 29(1-2):e1695, 2019.
- [52] Mike Papadakis and Yves Le Traon. Effective fault localization via mutation analysis: A selective mutation approach. In *Proceedings of the 29th annual ACM symposium on applied computing*, pages 1293–1300, 2014.
- [53] Seokhyeon Moon, Yunho Kim, Moonzoo Kim, and Shin Yoo. Ask the mutants: Mutating faulty programs for fault localization. In *2014 IEEE Seventh International Conference on Software Testing, Verification and Validation*, pages 153–162. IEEE, 2014.
- [54] Weijun Shen, Jun Wan, and Zhenyu Chen. Munn: Mutation analysis of neural networks. In *2018 IEEE international conference on software quality, reliability and security companion (QRS-C)*, pages 108–115. IEEE, 2018.
- [55] Jie M Zhang, Mark Harman, Lei Ma, and Yang Liu. Machine learning testing: Survey, landscapes and horizons. *IEEE Transactions on Software Engineering*, 48(1):1–36, 2020.
- [56] Florian Tambon, Foutse Khomh, and Giuliano Antoniol. A probabilistic framework for mutation testing in deep neural networks. *Information and Software Technology*, 155:107129, 2023.
- [57] Zan Wang, Hanmo You, Junjie Chen, Yingyi Zhang, Xuyuan Dong, and Wenbin Zhang. Prioritizing test inputs for deep neural networks via mutation analysis. In *2021 IEEE/ACM 43rd International Conference on Software Engineering (ICSE)*, pages 397–409. IEEE, 2021.
- [58] Xueqi Dang, Yinghua Li, Mike Papadakis, Jacques Klein, Tegawendé F Bissyandé, and Yves Le Traon. Graphprior: mutation-based test input prioritization for graph neural networks. *ACM Transactions on Software Engineering and Methodology*, 33(1):1–40, 2023.
- [59] Jingyi Wang, Guoliang Dong, Jun Sun, Xinyu Wang, and Peixin Zhang. Adversarial sample detection for deep neural network through model mutation testing. In *2019 IEEE/ACM 41st International Conference on Software Engineering (ICSE)*, pages 1245–1256, 2019.
- [60] Rhiannon Michelmores, Matthew Wicker, Luca Laurenti, Luca Cardelli, Yarin Gal, and Marta Kwiatkowska. Uncertainty quantification with statistical guarantees in end-to-end autonomous driving control. In *2020 IEEE international conference on robotics and automation (ICRA)*, pages 7344–7350. IEEE, 2020.